Review

Christina Krempl, Daniela Lazzaretti and Remco Sprangers*

A structural biology view on the enzymes involved in eukaryotic mRNA turnover

https://doi.org/10.1515/hsz-2023-0182
Received April 13, 2023; accepted August 24, 2023;
published online September 15, 2023

Abstract: The cellular environment contains numerous ribonucleases that are dedicated to process mRNA transcripts that have been targeted for degradation. Here, we review the three dimensional structures of the ribonuclease complexes (Pan2-Pan3, Ccr4-Not, Xrn1, exosome) and the mRNA decapping enzymes (Dcp2, DcpS) that are involved in mRNA turnover. Structures of major parts of these proteins have been experimentally determined. These enzymes and factors do not act in isolation, but are embedded in interaction networks which regulate enzyme activity and ensure that the appropriate substrates are recruited. The structural details of the higher order complexes that form can, in part, be accurately deduced from known structural data of subcomplexes. Interestingly, many of the ribonuclease and decapping enzymes have been observed in structurally different conformations. Together with experimental data, this highlights that structural changes are often important for enzyme function. We conclude that the known structural data of mRNA decay factors provide important functional insights, but that static structural data needs to be complemented with information regarding protein motions to complete the picture of how transcripts are turned over. In addition, we highlight multiple aspects that influence mRNA turnover rates, but that have not been structurally characterized so far.

Keywords: conformational changes; deadenylation; exoribonuclease; mRNA decapping; mRNA turnover

***Corresponding author: Remco Sprangers**, Institute of Biophysics and Physical Biochemistry, Regensburg Center for Biochemistry, University of Regensburg, D-93053 Regensburg, Germany, E-mail: remco.sprangers@ur.de. https://orcid.org/0000-0001-7323-6047
Christina Krempl and Daniela Lazzaretti, Institute of Biophysics and Physical Biochemistry, Regensburg Center for Biochemistry, University of Regensburg, D-93053 Regensburg, Germany. https://orcid.org/0000-0002-5372-9343 (D. Lazzaretti)

1 Introduction

The abundance of cellular bio-molecules is determined by the relative rates of synthesis and degradation. For eukaryotic mRNAs, synthesis is a complex hierarchical and multi-step process that sequentially involves RNA polymerase II mediated transcription, 5′ m^7G capping, 3′ polyadenylation, splicing, export from the nucleus and, in many cases, base editing. Two main features protect mRNA transcripts against rapid and uncontrolled degradation: the 5′ m^7G cap structure, that blocks access for the exoribonuclease Xrn1, as well as a 3′ poly(A) tail, that associates with one or multiple copies of the poly(A) binding protein (Pab1). Both elements serve multiple purposes and are e.g. also important for efficient translation.

The simplest form of the protecting m^7G mRNA cap structure (termed cap0) consists of an N7-methylated guanosine that is connected to the 5′ end of the mRNA by a 5′–5′ triphosphate bridge (Shatkin 1976). The ribose 2′ OH group of the most 5′ RNA base is often methylated to form the cap1 structure. 2′ O-methylations of the following riboses result in the formation of cap2 to cap4 structures, where mRNA with a cap2 appears to have a mildly increased stability compared to cap1 mRNA (Despic and Jaffrey 2023) by a mechanism that remains elusive. The downstream bases in the mRNA body may also be modified in a wide range of manners, which can influence mRNA stability in multiple ways (Boo and Kim 2020), through molecular mechanisms that are not yet fully understood. Given the pivotal role of the cap in mRNA metabolism, it is desirable to make use of capped RNA in biochemical and structural studies, which can easily be produced *in vitro* using the capping enzyme complex from the vaccinia virus (Fuchs et al. 2016).

The length of the mRNA-protecting poly(A) tail ranges from 70 to 80 nucleotides in yeast to over 250 nucleotides in mammalian cells (Lima et al. 2017). Additionally, the length of the poly(A) tail differs between transcripts, and developmental, differentiation and cell cycle dependent stages, and has important implications for cellular function (Jalkanen et al. 2014). The 3′ poly(A) tail generally interacts specifically with Pab1, that thereby protects the 3′ end of the transcript against rapid exonucleolytic degradation (Eckmann et al. 2011; Mangus et al. 2003).

The half-lives of different mRNAs vary significantly, from 3 min to over 90 min in yeast (Wang et al. 2002), and can be even longer in human cells (Yang et al. 2003). These large variations in mRNA decay rates can in part be attributed to poly(A) tail length, but also depend on specific sequence elements (e.g. AU-rich elements in the 3′ UTR) or abnormalities in the transcript that can influence degradation rates significantly (Kurosaki et al. 2019; Xu et al. 1997). Generally, mRNA turnover is initiated by the stepwise shortening of the 3′ poly(A) tail (deadenylation), and proceeds through the action of decapping enzymes that remove the protecting mRNA cap structure and 5′→3′ or 3′→5′ exoribonucleases that degrade the transcript processively from either end.

Below, we describe the structural details of the Pan2-Pan3 and Ccr4-Not deadenylation complexes and of the 5′→3′ and 3′→5′ mRNA decay pathways. Known structures of the different sub-complexes depicted here originate from different species (e.g. human or yeast). Importantly, these complexes are highly conserved and their core structures appear to be species-independent. However, there is considerable variation in the details of the interaction between the sub-complexes and the mechanism through which additional factors are recruited.

2 mRNA turnover step 1: deadenylation by Pan2-Pan3

For canonical mRNA turnover, the degradation of the transcript is generally initiated by a two-step shortening of the 3′ poly(A) tail, which is often the rate limiting step in mRNA decay. As long as the poly(A) tail is long enough to interact with at least two copies of Pab1, the transcript is shortened by the 200–230 kDa Pan2-Pan3 complex (Brown and Sachs 1998; Schäfer et al. 2019). Multiple structures of Pan2, Pan3, and complexes thereof have been determined (Table 1), providing important insights into the mechanism of Pan2-Pan3-mediated deadenylation.

The C-terminus of the Pan2 protein contains a catalytically active distributive exoribonuclease (RNase) domain (Figure 1), which implies that the active site of the complex dissociates from the substrate between successive deadenylation steps (Lowell et al. 1992). Pan2 activity is enhanced by its cofactor Pan3 that contains a Pab1-interacting motif 2 (PAM-2 motif) (Uchida et al. 2004; Wolf et al. 2014). This motif binds specifically to the PABC domain of Pab1 and thereby ensures the recruitment of the Pan2-Pan3 complex to mRNA substrates with longer poly(A) tails (Siddiqui et al. 2007). In addition, Pan3 interacts with tryptophan-rich stretches in TNRC6/GW182 (Christie et al. 2013; Fabian et al. 2011), a protein that is central in the miRNA-mediated mRNA decay pathway. This exemplifies a strategy that is often exploited in mRNA turnover, where the mRNA degradation machinery is recruited to specific transcripts that have been designated for degradation through different pathways.

In isolation, Pan3 forms an almost symmetric homodimer, with a kink in one of the two central coiled-coil domains (Christie et al. 2013). This slight asymmetry favours the association of a single copy of Pan2, mediated by

Table 1: Structures of the Pan2-Pan3 complex.

PDB ID	Pan2	Pan3	Other
4CZW (Jonas et al. 2014)	n.c. UCH, RNase		
4CZV (Jonas et al. 2014)	n.c. WD40		
4Q8H (Schäfer et al. 2014)	s.c. UHC, RNAse		
4Q8G (Schäfer et al. 2014)	s.c. UHC		
6R9I (Tang et al. 2019)	s.c. UCH, RNase		
6R9J, M, O, P, Q (Tang et al. 2019)	s.c. UHC, RNase		Different RNA substrates
4BWK, 4BWX (Christie et al. 2013)		n.c. PK, CC, CK	
4BWP (Christie et al. 2013)		d.m. PK, CC, CK	
4CYI (Wolf et al. 2014)		c.t. PK, CC, CK	
4CYK (Wolf et al. 2014)		c.t. ZF	
4CYJ (Wolf et al. 2014)	c.t. Linker	c.t. PK, CC, CK	
4D0K (Jonas et al. 2014)	c.t. WD40	c.t. CK	
4CZX, (Jonas et al. 2014)	n.c. WD40	n.c. CK	
4CZY (Jonas et al. 2014)	n.c. WD40	n.c. PK, CC, CK	
4XR7 (Schäfer et al. 2014)	s.c. UCH, RNase	s.c. PK, CC, CK	
6R5K (Schäfer et al. 2019)	s.c.	s.c. PK, CC, CK	3 copies of Pab1

Abbreviations: s.c., *Saccharomyces cerevisiae*; c.t., *Chaetomium thermophilum*; n.c., *Neurospora crassa*; UCH, ubiquitin C-terminal hydrolase (Pan2); RNase, DEDD superfamily 3′→5′ exo-RNase domain (Pan2); WD40, WD40 domain (Pan2); CK, C-terminal knob domain (Pan3); CC, coiled coil (Pan3); PK, pseudokinase domain (Pan3); ZF, Zinc-Finger (Pan3).

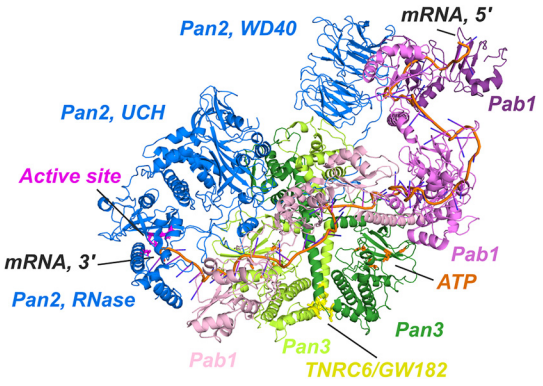

Figure 1: Structure of the Pan2-Pan3 complex. One Pan2 (blue) protein interacts with an asymmetric Pan3 dimer (light and dark green). The 3′ end of the mRNA (orange) interacts with the Pan2 active site (magenta). The upstream bases interact with three Pab1 proteins (light pink, pink and violet). Pan3 contains interaction sites for ATP (orange) and for TNRC6/GW182 (yellow). The figure is based on a superposition of the structures in PBD IDs 6R5K and 4BWP (Table 1).

an over 100 amino acid long linker region (Schäfer et al. 2014; Wolf et al. 2014) and the WD40 domain (Jonas et al. 2014) of the Pan2 enzyme (Figure 1). The mRNA substrate is then recognized by the Pan2-Pan3 complex through at least three independent interactions. First, the active site of Pan2 specifically recognizes the unique stacked helical A-form structure that poly(A) RNA adopts (Tang et al. 2019), without forming specific interactions with the adenine bases. Second, the far N-terminal region of Pan3 contains a Zinc-Finger that enhances the interactions with the substrate (Wolf et al. 2014). Finally, the poly(A) substrate is recruited to the Pan2-Pan3 complex via Pab1, as is visualized in the impressive structure of a Pan2-Pan3-Poly(A)-Pab1 complex (Schäfer et al. 2019), where two to three copies of Pab1 exploit one surface to interact specifically with Pan2 and Pan3 and another surface to simultaneously interact with the poly(A) sequence in the substrate. These data also provide a mechanistic explanation for the inefficiency of Pan2-Pan3 in degrading RNA substrates with short poly(A) tails that interact with less than two Pab1 proteins, and for the stimulatory effect exerted by Pab1 on Pan2-Pan3 catalytic activity (Schäfer et al. 2019).

Importantly, the Pan2-Pan3 domain orientations and interactions in multiple independent sub-complexes from different organisms (Table 1) superpose well on the structure of the full complex (Figure 1). This highlights that the structural biology bottom-up approach, where smaller subassemblies are studied in isolation, is able to provide relevant structural and mechanistic insights into the full Pan2-Pan3 assembly. Nevertheless, highly dynamic regions often remain unresolved, especially in atomic models obtained from cryo-electron microscopy and X-ray crystallography. For the Pan2-Pan3 complex, over 200 residues of the N-terminal region of Pan3, including the Zinc-Finger and the PAM-2 motif, are invisible. It thus remains unclear how these elements function in the regulation of the deadenylation process. Furthermore, the static images of the active Pan2-Pan3 complex are unable to reveal how the poly(A) tail is translocated towards the active site during deadenylation. The slow nature of the Pan2-Pan3-mediated deadenylation might in that regard be correlated with the very large intermolecular interface between the substrate and the Pan2-Pan3-Pab1 complex, where many interactions need to be broken to shift the substrate towards the active site.

3 mRNA turnover step 2: deadenylation by the Ccr4-Not complex

After Pan2-Pan3 has shortened the poly(A) tail to less than 25–110 nucleotides (Decker and Parker 1993; Yamashita et al. 2005), the second step in deadenylation is performed by the multi-subunit Ccr4-Not complex (Tucker et al. 2001; Yamashita et al. 2005) that contains the catalytically active exonuclease CNOT7/Caf1/Pop2 and the deadenylase CNOT6/Ccr4.

The core of the Ccr4-Not complex is the CNOT1/Not1 protein (267 kDa in humans/240 kDa in yeast), which contains multiple consecutive helical domains connected by linker regions that are likely unstructured and flexible (Figure 2) (Raisch et al. 2019). The Not1 protein acts as a scaffold for interactions with other subunits of the Ccr4-Not complex (Figure 2; Table 2) to assemble a complex that has a molecular weight of around 670 kDa (in humans). From N- to C-terminus, the protein can be roughly divided into four different modules.

First, the NOT1-N module contains an N-terminal Not1 MIF4G domain (middle portion of eIF4G, termed N-MIF4G here), a number of N-terminal helix-turn-helix HEAT (Huntingtin, elongation factor 3, protein phosphatase 2A, and the yeast kinase TOR1) repeats (termed N-HEAT here) and several middle HEAT repeats (termed M-HEAT here). This N-terminal region of Not1 interacts with the mammalian factors CNOT10 and CNOT11 to form an RNA-interacting module, termed the NOT1-N module, that enhances deadenylase activity (Raisch et al. 2019) through an unknown mechanism. The structure of the NOT1-N module (Mauxion et al. 2023) shows an intertwined core, composed of all three proteins, and a flexibly attached so-called antenna that consists of the CNOT11 C-terminal domain. This C-terminal domain of CNOT11 is a binding hub for factors that can be

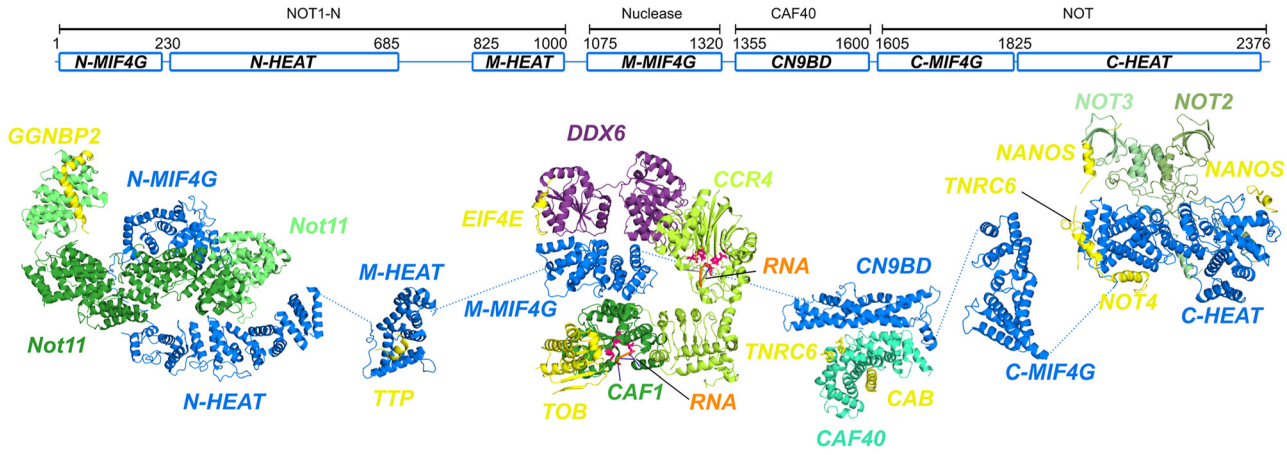

Figure 2: Structural model of the Ccr4-Not complex. The domain organization of the scaffold protein CNOT1 (top), where residue numbers refer to the approximate domain boundaries in the human protein. The four modules form more or less independently structured units that are connected via linker regions. For the NOT1-N module, PDB IDs 8BFI and 8BFJ have been superposed (Table 2), while the TTP complex is based on PDB ID 4J8S. For the nuclease module, (parts of) the PDB IDs 4B8C, 3NGO, 2D5R, 5ANR and 2A1R have been superposed. For the Caf40 module, PDBI Ds 4CRV, 5ONA, 5LSW and 6HOM have been superposed. For the NOT module, PDB IDs 4C0D, 4CQO, 5FU7, 5AJD and 6H3Z have been superposed. The Not1 protein is shown in blue, other Ccr4-Not factors are coloured in different shades of green (with active sites highlighted in magenta), Ccr4-Not-associated proteins are in yellow, and RNA is shown in orange.

Table 2: Structures of the Ccr4-Not complex.

PDB ID	Not1	Not10	Not11	Caf1	Ccr4	Caf40/Not9	Not2	Not3	Other
8BFI, 8BFJ (Mauxion et al. 2023)	h.s. N-MIF4G N-HEAT	h.s.	h.s.						h.s. GGNBP2
4B8B (Basquin et al. 2012)	c.s. N-HEAT M-HEAT								
4J8S (Fabian et al. 2013)	h.s. M-HEAT								h.s. TTP
4B8C (Basquin et al. 2012)	s.c. M-MIF4G			s.c. ND	s.c.				
4B8A (Basquin et al. 2012)	c.s. M-MIF4G			s.c. ND					
4GMJ (Petit et al. 2012)	h.s. M-MIF4G			h.s. ND					
2A1R (Wu et al. 2005)					h.s. PARN				$(A)_3$
7VOI (Zhang et al. 2022)	h.s. M-MIF4G			hs. ND	h.s. ND				
7AX1 (Chen et al. 2021)				h.s. nd	h.s. nd				
3NGO (Wang et al. 2010)					h.s. ND				$(A)_4$ DNA
2D5R (Horiuchi et al. 2009)				h.s. ND					h.s. TOB
4CT4 (Mathys et al. 2014)	h.s. M-MIF4G								h.s. DDX6

Table 2: (continued)

PDB ID	Not1	Not10	Not11	Caf1	Ccr4	Caf40/Not9	Not2	Not3	Other
5ANR (Ozgur et al. 2015)	h.s. M-MIF4G								h.s. DDX6, Eif4e
4CRW (Chen et al. 2014)	h.s. M-MIF4G								h.s. DDX6
4CRV, 4CRU (Chen et al. 2014)	h.s. CN9BD					h.s.			h.s. TRP
4CT6, 4CT7 (Mathys et al. 2014)	h.s. CN9BD					h.s.			h.s. TRP
4CV5 (Mathys et al. 2014)	s.c. CN9BD					s.c.			
5ONA (Sgromo et al. 2018)	h.s. CN9BD					h.s.			d.m. Bag-of-marbles
5LSW (Sgromo et al. 2017)						h.s.			d.m. Roquin
6HOM, 6HON (Keskeny et al. 2019)						h.s.			d.m. Not4
6H3Z (Raisch et al. 2018)	c.t. C-MIF4G								
4C0D (Boland et al. 2013)	h.s. C- HEAT						h.s.	h.s.	
4BY6 (Bhaskar et al. 2013)	s.c. C-HEAT						s.c.	s.c. Not5	
4CQO (Bhandari et al. 2014)	h.s. C-HEAT								h.s. Nanos
5FU6, 5FU7 (Raisch et al. 2016)	h.s. C-HEAT						h.s.	h.s.	D.m. Nanos
5AJD (Bhaskar et al. 2015)	s.c. C-HEAT								s.c. Not4
6TB3 (Buschauer et al. 2020)								s.c. Not5	Ribosome

Abbreviations: h.s., *Homo sapiens*; s.c., *Saccharomyces cerevisiae*; c.t., *Chaetomium thermophilum*; d.m., *Drosophila melanogaster*; PARN, Poly(A)-specific ribonuclease that is structurally related to Caf1.

recruited to the Ccr4-Not complex, including the tumour repressor protein GGNBP2 (gametogenetin-binding protein 2) (Mauxion et al. 2023). The M-HEAT repeats that follow the CNOT1-CNOT10-CNOT11 unit have also been structurally characterized and interact with the protein TTP (tristetraprolin) (Fabian et al. 2013), mediating the direct recruitment of the Ccr4-Not complex to mRNAs with destabilizing AU-rich elements (Figure 2). The M-HEAT region of the yeast Not1 protein appears to interact stably with the rest of the NOT1-N module (Basquin et al. 2012). This part of Not1 is not present in the structure of the human NOT-N module and it is thus not clear, whether the stable association of the M-HEAT region with the NOT-N module is conserved.

The second module in the Ccr4-Not complex is the nuclease module, that is built around the CNOT1 middle MIF4G domain (termed M-MIF4G here). This M-MIF4G domain binds to the exoribonuclease CNOT7/Caf1/pop2, which in turn recruits the deadenylase CNOT6/Ccr4. The latter is the only component of the Ccr4-Not complex that does not directly interact with the Not1 scaffold protein (Basquin et al. 2012). Caf1 and Ccr4 are structurally distinct ribonucleases: like Pan2, Caf1 belongs to the DEDDh family of nucleases, whereas Ccr4 belongs to the heterogeneous EEP (exonuclease-endonuclease-phosphatase) family of phosphoesterases. Both nucleases have a strong preference for poly(A) RNA with a 3′ OH adenine residue (Chen et al. 2021), which has been

structurally visualized for Ccr4 (Wang et al. 2010). Even though both ribonuclease activities are in principle redundant, both are required to achieve a fully functional deadenylation complex in cells (Piao et al. 2010). Biochemically, it has been observed that the Ccr4-Not activity is efficiently blocked when two or more non-adenine nucleotides are present (Raisch et al. 2019), which prevents non-specific RNA degradation. Single non-adenine bases are tolerated, and mainly removed by Caf1 (Chen et al. 2021). Interestingly, even non-adenine bases up to two nucleotides from the free 3′ end are detected and result in a slowdown of deadenylation (Chen et al. 2021), suggesting a complex mechanism that tunes the mRNA decay speed and thus mRNA stability. The relative orientation of the Not1 M-MIF4G domain and Caf1 appears invariant, as both domains adopt the same orientation in multiple crystal structures (Basquin et al. 2012; Petit et al. 2012; Zhang et al. 2022). The orientation of Caf1 and Ccr4, on the other hand, is not fixed, as these domains have been observed in different relative orientations (Chen et al. 2021; Zhang et al. 2022). This structural plasticity might relate to the way both nuclease active sites act together. It is tempting to speculate that the Ccr4 and Caf1 proteins rotate when e.g. non-adenine bases are encountered in the substrate, given the different degree of inhibition displayed in the presence of distinct non-adenine bases by the two nucleases (Chen et al. 2021) and the loss of the helical structure that a pure poly(A) RNA adopts (Tang et al. 2019). The second function of the M-MIF4G domain in the nuclease module is the recruitment of the DEAD box helicase DDX6/Dhh1 that links the Ccr4-Not complex to mRNA decapping (see below) and translational repression (Chen et al. 2014; Mathys et al. 2014; Ozgur et al. 2015). The M-MIF4G domain of Not1 induces an active conformation in the DDX6 helicase, which is important for efficient miRNA repression (Mathys et al. 2014). A superposition of the available structures reveals that the DDX6 helicase is in close spatial proximity to the nuclease domains (Figure 2). It is, however, still unclear whether DDX6 helicase activity stimulates deadenylation, and if such stimulation would be achieved actively, through the unwinding of secondary structure elements in the mRNA, or passively, by providing an additional RNA binding platform. Additionally, the nuclease module interacts, through Caf1, with the TOB family of antiproliferative proteins (Horiuchi et al. 2009; Hosoda et al. 2011), thereby linking the deadenylation complex to cell cycle regulation and providing a mechanism through which specific RNAs can be recruited to the deadenylase complex.

The Ccr4-Not nuclease module is followed by the Caf40 module that consists of the Not1 CNOT9-binding domain (CN9BD) and the CNOT9/Caf40 (Chen et al. 2014; Mathys et al. 2014). On the one hand, CNOT9 can interact with Trp rich sequences, and thereby bind the TNRC6/GW182 protein, enabling direct recruitment of the Ccr4-Not complex to miRNA targets (Chen et al. 2014; Mathys et al. 2014). On the other hand, Caf40 directly interacts with proteins that contain a Caf40-binding motif (CAB) that is present in e.g. the *Drosophila* protein Bag-of-marbles (Sgromo et al. 2018), in a number of Roquin proteins (Sgromo et al. 2017), and in metazoan Not4, a conserved E3 ubiquitin ligase (Keskeny et al. 2019). These interactions either target specific mRNAs to the Ccr4-Not complex, or facilitate ubiquitylation of multiple substrates, including ribosome-associated factors.

Finally, the C-terminal Not1 MIF4G-HEAT repeat domains interact with Not2 and Not3 (or the paralogous protein Not5) to form the Not module (Bhaskar et al. 2013; Boland et al. 2013). This module recruits the Ccr4-Not complex to numerous specific mRNA transcripts, including miRNA targets and AU-rich element-containing mRNAs such as the transcription regulator Nanos (Bhandari et al. 2014; Raisch et al. 2016). Even though the structure of the core C-terminal Not module is conserved, the interaction surface of recruited proteins can differ between vertebrates and invertebrates as it is observed for e.g. Nanos. Likewise, yeast Not4 interacts differently with the metazoan and the yeast Ccr4-Not complex, as in the former case interaction is mediated by Caf40 (see above), and in the latter the Not module directly binds Not4 (Bhaskar et al. 2015). Yeast Not5 and its human orthologue CNOT3 can interact directly with stalling ribosomes and thereby target transcripts with non-optimal codon usage for degradation (Absmeier et al. 2022; Buschauer et al. 2020). The exoribonuclease Xrn1 (see below) has also been shown to interact with the Not module (Chang et al. 2019), though the structural details of the interaction are still unknown. This interaction inhibits the Caf1-mediated deadenylation activity of the Ccr4-Not complex (Chang et al. 2019) and thus reveals a mechanism that regulates the interplay of deadenylation and 5′→3′ transcript degradation. Finally, the Not module specifically interacts with poly(U) RNA in a structurally undetermined manner (Bhaskar et al. 2013).

Despite the abundant structural information on the isolated modular components of the Ccr4-Not complex (Figure 2), it remains unclear how these building blocks are assembled in three dimensional space. A low resolution electron microscopy map indicates that the modules are arranged into an L-shaped complex (Nasertorabi et al. 2011) where the relative positioning of the arms varies between reconstructions, suggesting flexibility. It is thus plausible that the full complex is highly dynamic in solution, which would explain the observed cross-talk between different modules and which could provide additional means of regulating activity and/or substrate recruitment. This flexibility, however, results in challenges in the determination of higher resolution structures of the complete assembly

(Raisch et al. 2019). In that light, it is worth mentioning that it is not possible to simply superpose the structures of the individual Not modules onto AlphaFold-derived models (Jumper et al. 2021) of the full length Not1 protein from either yeast or humans, as this results in severe structural clashes between the modules. This computational exercise underscores the importance of experimental methods to obtain information on highly complex assemblies as relative domain orientations are not well-predictable.

4 mRNA turnover step 3

After 3′ deadenylation, the mRNP (messenger ribonucleoprotein) complex undergoes a transition from a translationally competent state to one that is primed for rapid and irreversible transcript degradation (Tharun and Parker 2001). This mRNA decay process can occur via either of two pathways (Garneau et al. 2007). One involves 5′ mRNA decapping by the Dcp2 enzyme, followed by the processive 5′→3′ exoribonucleolytic hydrolysis of the mRNA body by Xrn1. Alternatively, the transcript can be degraded in the 3′→5′ direction by the cytoplasmic RNA exosome complex, followed by decapping of the residual small mRNA fragment by the scavenger decapping enzyme DcpS. Mechanistically, these pathways can have a different functional consequence, as the decapping of a transcript results in an immediate inhibition of translation initiation and thus prevents the production of truncated proteins that could still occur in the 3′→5′ degradation pathway. It is still unknown how an mRNA is committed to either of these decay pathways. Nevertheless, it is plausible to postulate that this step, like all other steps in mRNA turnover, is tightly regulated.

4.1 mRNA turnover step 3a: Xrn1-mediated degradation of the mRNA body

The 5′→3′ mRNA degradation pathway appears to be the most prominent one in yeast (Muhlrad et al. 1995). Over the years, a large number of structures of the components involved in this pathway have been elucidated (Table 3). Nevertheless, the exact molecular and structural details that result in the recruitment of the 5′ decapping machinery to the 3′ deadenylated mRNA remain unclear. Based on the knowledge gathered from sub-complexes, it is possible to obtain insights into the structural links between deadenylation, decapping and exonucleolytic degradation of the mRNA body.

Table 3: Structures of proteins involved in 5′→3′ mRNA decay.

PDB ID	Xrn1	Dcp1	Dcp2	Edc1	Edc3	Pat1	Dhh1	Lsm1-7	Other	RNA
2Y35 (Jinek et al. 2011)	d.m.									DNA
3PIE, 3PIF (Chang et al. 2011)	k.l. E178Q									
6Q8Y (Tesina et al. 2019)	s.c.								Ribosome	mRNA
2LYD (Braun et al. 2012)	d.m. IDR	d.m.								
1Q67 (She et al. 2004)		s.c.								
2WX3 (Tritschler et al. 2009a)		h.s. CTD								
4B6H (Lai et al. 2012)		h.s.							PNRC2	
2WX4 (Tritschler 2009a)		d.m.								
5MP0, 5QOH-5QOZ, 5QP0-5QP9, 5QPA-5QPC			h.s. CD						Inhibitors	

Table 3: (continued)

PDB ID	Xrn1	Dcp1	Dcp2	Edc1	Edc3	Pat1	Dhh1	Lsm1-7	Other	RNA
2A6T (She et al. 2006)			s.p. RD, CD							
2JVB (Deshmukh et al. 2008)			s.c. CD							
4K6E, 4KG3, 4KG4 (Aglietti et al. 2013)			s.c. ND							
2QKL, 2QKM (She et al. 2008)		s.p.	s.p. RD							+/− ATP
5LON (Charenton et al. 2016)		k.l.	k.l. RD, CD							
5J3Y (Valkov et al. 2016)		s.p.	s.p. RD, CD							
5KQ1 (Mugridge et al. 2016)		s.p.	s.p. RD, CD						h.s. PNRC2	
5KQ4 (Mugridge et al. 2016)		s.p.	s.p. RD, CD						h.s. PNRC2	Cap analogue
5J3Q (Valkov et al. 2016)		s.p.		s.p.						
5JP4 (Wurm et al. 2016)		s.p.		s.p.						
5N2V (Wurm et al. 2017)		s.p.	s.p. RD, CD	s.p.						m^7Gpp
5J3T (Valkov et al. 2016)		s.p.	s.p. RD, CD	s.p.						
6AM0 (Mugridge et al. 2018)		k.l.	k.l. RD, CD	k.l.	k.l. LSm					Cap analogue
5LOP (Charenton et al. 2016)		k.l.	k.l. RD, CD		k.l. LSm					m^7GDP
4A54 (Fromm et al. 2012)			s.p. HLM		s.p. LSm					
5LM5, 5LMF, 5LMG (Charenton et al. 2017)			s.c. HLMs			s.c. CTD				
6Y3Z (Charenton et al. 2020)		s.c.	s.c.		s.c. LSm				s.c. Pby1	
6Y3P (Charenton et al. 2020)									k.l. Pby1	
2RM4 (Tritschler et al. 2007)					d.m. LSm					
2VC8 (Tritschler et al. 2007)					h.s. LSm					
3D3J, 3D3K (Ling et al. 2008)					h.s. YjeF-N					
4A53 (Fromm et al. 2012)					s.p. Lsm					

Table 3: (continued)

PDB ID	Xrn1	Dcp1	Dcp2	Edc1	Edc3	Pat1	Dhh1	Lsm1-7	Other	RNA
4OGP, 4OJJ (Fourati et al. 2014)						s.c. CTD				
2XEQ, 2XER, 2XES (Braun et al. 2010)						h.s. CTD				
1S2M (Cheng et al. 2005)							s.c.			
2WAX, 2WAY (Tritschler et al. 2009a)					h.s. FDF		h.s. RecA2			
4BRU (Sharif et al. 2013)					s.c. FDF		s.c. RecA2			
4BRW (Sharif et al. 2013)						s.c. N-IDR	s.c. RecA2			
6S8S (Peter et al. 2019)					h.s. FDF		h.s. RecA2			
6F9S (Brandmann et al. 2018)							h.s. RecA2		c.e. Lsm14	
5ANR (Ozgur et al. 2015)							h.s. RecA2		h.s. CNOT1	
2VXG (Jinek et al. 2008)									d.m. Ge-1	
4Q2S (Fromm et al. 2014)									s.p. Pdc1	
4N0A (Wu et al. 2014)						s.c. CTD		s.c. Lsm2,3		
4C8Q (Sharif and Conti 2013)						s.c. CTD		s.c. Lsm1-7		
4C92 (Sharif and Conti 2013)								s.c. Lsm1-7		
4EMG (Wu et al. 2012)								s.p. Lsm3		
3BW1 (Naidoo et al. 2008)								s.c. Lsm3		
4EMK (Wu et al. 2012)								s.p. Lsm5,6,7		
3SWN (Mund et al. 2011)								s.p. Lsm5,6,7		
4M75 (Zhou et al. 2014)								s.c. Lsm1-7		
6PPQ, 6PPV (Montemayor et al. 2020)								s.p. Lsm1-7		RNA
4EMH (Wu et al. 2012)								s.p. Lsm4		

Abbreviations: h.s., *Homo sapiens*; s.p., *Schizosaccharomyces pombe*; s.c., *Saccharomyces cerevisiae*; d.m., *Drosophila melanogaster*; k.l., *Kluyveromyces lactis*; c.e., *Caenorhabditis elegans*; CTD, C-terminal domain (Dcp1, Pat1); RD, regulatory domain (Dcp2); CD, catalytic domain (Dcp2); HLM, helical leucine rich motif (Dcp2); Lsm, Lsm domain (Edc3); RecA2, second RecA domain (DDX6/Dhh1); N-IDR, N-terminal IDR (Pat1).

Table 4: Structures of proteins involved in 3′→5′ mRNA decay.

PDB ID	DcpS	Exo9	Rrp44/Dis3	Other	RNA/cap analogue
1VLR (Han et al. 2005)	m.m.				
6GBS (Fuchs et al. 2020)	c.t				
3BL7, 3BL9, 3BLA (Singh et al. 2008)	h.s.				Inhibitor
1ST0, 1ST4 (Gu et al. 2004)	h.s.				m^7GpppG, m^7GpppA
1XMM (Chen et al. 2005)	h.s.				m^7GDP
1XML (Chen et al. 2005)	h.s.				
4QDE, 4QEB, 4QDV (Hett et al. 2015)	h.s.				Inhibitor
6TRQ (Fuchs et al. 2020)	s.c.				m^7GpppGU
5OSY (Wojtczak et al. 2018)	h.s.				m^7G(5′S)ppSp(5′S)G
5BV3 (Neu et al. 2015)	s.c.				m^7GDP
7TUV (Cesaro et al. 2023)			t.b. CSDs-RNB-S1, open		RNA: GGUU
6MD3 (Cesaro et al. 2019)			t.b. PIN domain		
2VNU (Lorentzen et al. 2008)			s.c. CSDs-RNB-S1, open		RNA: $(A)_{10}$
4RO1 (Lv et al. 2015)			s.p. DIS3-like 2		
4PMW (Faehnle et al. 2014)			m.m. Dis3-like 2, open		RNA: $(U)_{14}$
2WP8 (Bonneau et al. 2009)		s.c Rrp41-Rrp45	s.c.		
2NN6 (Liu et al. 2006)		h.s.			
4OO1 (Wasmuth et al. 2014)		s.c.		s.c. Rrp6	RNA: $(A)_{24}$
5OKZ (Falk et al. 2017)		s.c.		s.c. Mpp6	
6H25 (Gerlach et al. 2018)		h.s.	h.s. Open	h.s. Mpp6	RNA: $(U)_{44}$
5JEA (Kowalinski et al. 2016)		s.c.	s.c. Closed	s.c. Ski7	RNA: 46 nt
5G06 (Liu et al. 2016)		s.c.	s.c. Open	s.c. Ski7	
5K36 (Zinder et al. 2016)		s.c.	s.c. Open	s.c. Rrp6	RNA: 17 nt

Table 4: (continued)

PDB ID	DcpS	Exo9	Rrp44/Dis3	Other	RNA/cap analogue
4IFD (Makino et al. 2013)		s.c.	s.c. Closed	s.c. Rrp6	RNA: 45 nt
5C0X (Makino et al. 2015)		s.c.	s.c. Closed	s.c. Rrp6	RNA: 45 nt (including a hairpin)
5VZJ (Wasmuth et al. 2017)		s.c.	s.c. Open	s.c. Rrp6, Mpp6	RNA: 11 nt RNA: 19 nt
5C0W (Makino et al. 2015)		s.c.	s.c. Open	s.c. Rrp6, Rrp47	RNA: 18 nt
6D6Q, 6D6R (Weick et al. 2018)		h.s.	h.s. Open	h.s. Rrp6, Mpp6, Mtr4	RNA: 62 nt
6FSZ (Schuller et al. 2018)		s.c.	s.c. Closed	s.c. Rrp6, Rrp47, Mtr4, Mpp6	RNA: 23 nt
6LQS (Du et al. 2020)		s.c.	s.c. Closed	s.c. Rrp6, Rrp47, Mtr4, Mpp6	RRNA and pre-90S ribosome
6FT6 (Schuller et al. 2018)				s.c. Rrp6, Rrp47, Mtr4, Mpp6	RRNA and pre-60S ribosome
4BUJ (Halbach et al. 2013)				s.c. Ski2, Ski3, Ski8	
7QDR, 7QDS (Kögel et al. 2022)				h.s. Ski2, Ski3, Ski8	
7QDY, 7QDZ (Kögel et al. 2022)				h.s. Ski2, Ski3, Ski8	RNA: $(U)_{25}$ or $(U)_6$
5MC6 (Schmidt et al. 2016)				s.c. Ski2, Ski3, Ski8	mRNA and ribosome
7QE0 (Kögel et al. 2022)				h.s. Ski2	RNA: $(U)_9$

Abbreviations: m.m., *Mus musculus*; c.t., *Chaetomium thermophilum*; h.s., *Homo sapiens*; t.b., *Trypanosoma brucei*; nt, nucleotides; CSD, Cold Shock Domain (Rrp44); RNB, catalytic domain of ribonuclease (Rrp44); S1, S1 domain (Rrp44). Note that Rrp6, Rrp47 (Exosome complex protein LRP1), Mtr4 and Mpp6 are nuclear proteins and exosome complexes that contain those subunits are thus not directly involved in canonical mRNA turnover. These complexes are included in this Table to illustrate the structural plasticity of Rrp44.

The 3′ end of the transcript interacts with the pore of the ~90 kDa heteroheptameric doughnut-shaped Lsm1-7 complex (Montemayor et al. 2020) (Figure 3A, red/black). The Lsm2 and Lsm3 subunits of this complex stably associate with the C-terminal helical region (Pat1-C) of the ~90 kDa multi-domain scaffolding protein PATL1/Pat1 (Sharif and Conti 2013; Wu et al. 2014) (Figure 3A). Pat1 binding enhances the affinity and specificity of the Lsm1-7 ring for oligoA RNA, as present in a deadenylated 3′ poly(A) mRNA. This interaction is mediated by the structurally uncharacterized middle domain of Pat1 (Pat1-M) (Lobel et al. 2019), the C-terminal domain of Pat1 (Pat1-C), and the C-terminal extension of Lsm1 (Chowdhury et al. 2007; Lobel and Gross 2020). It would be exciting to determine the structural details of this Lsm-Pat1-mRNA complex, and thus to understand the molecular mechanisms that result in the specific recognition of deadenylated transcripts. At the same time, the Pat-C region interacts with one of the multiple helical-rich motifs in the C-terminal IDR (Intrinsically Disordered Region) of the Dcp2 mRNA decapping enzyme (Charenton et al. 2017) (Figure 3A, green). Note that this C-terminal IDR is not present in human Dcp2 protein, where a long C-terminal IDR is instead present in the Dcp2-interacting protein Dcp1. Functionally, Pat1-C thus links recognition of the deadenylated 3′ end of a transcript (by Lsm1-7) to the hydrolysis of the 5′ mRNA cap structure (by Dcp2).

The 5′→3′ decay interaction network is significantly more extended as described above and involves multiple additional factors. The C-terminal IDR of Dcp2 (or Dcp1 in humans) can simultaneously recruit multiple Edc3 proteins via an N-terminal Lsm domain (Fromm et al. 2012) (Figure 3A, blue). These Edc3 proteins in turn dimerize through a C-terminal Yjef_N domain and exploit an internal IDR to interact with the

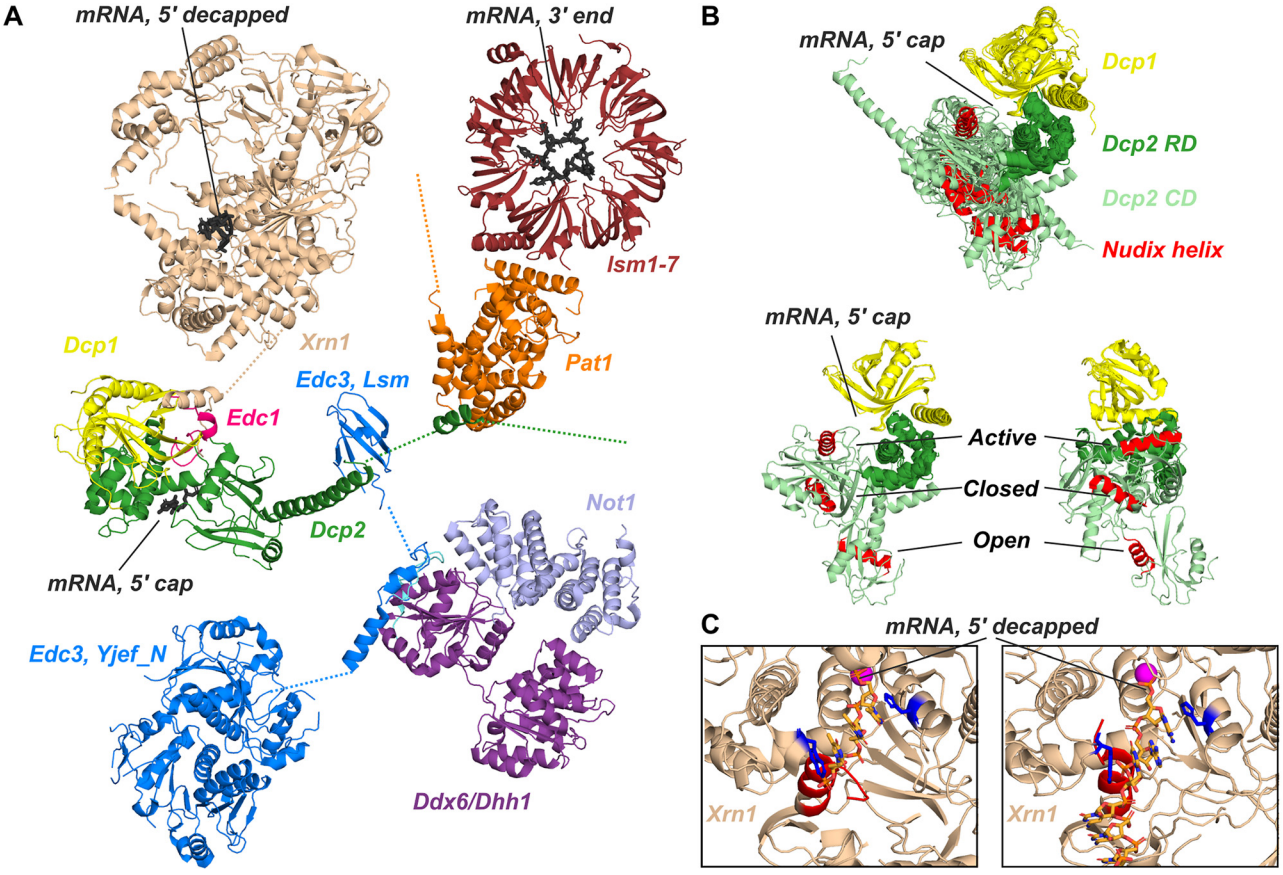

Figure 3: Structural link between 3′ deadenylation and 5′ decapping and degradation. (A) Superposition of known three-dimensional structures involved in 5′→3′ mRNA decay (Table 3). The Lsm1-7 complex (red) interacts with the 3′ end of the mRNA (black, PDB ID 6PPV) as well as with Pat1 (orange, PDB ID 4C8Q). Pat1 connects to Dcp2 (green, PDB ID 5LM5) via a number of linear motifs in its C-terminal IDR (only one of the interactions is shown). These motifs also interact with the Lsm domain in Edc3 (blue, PDB ID 6AM0). Edc3 dimerizes via a C-terminal Yjef_N domain (PDB ID 3D3J) and interacts through its central IDR with the DEAD box helicase DDX6/Dhh1 (purple, PDB ID 6S8S). This helicase also links the mRNA to the deadenylation machinery via Not1 (light blue, PDB ID 5ANR). The mRNA decapping enzyme Dcp2 interacts with the decapping activators Dcp1 (yellow) and Edc1 (pink; PDB ID 6AM0). Dcp1 interacts with the C-terminal IDR of Xrn1 (light brown, PDB ID 2LYD and 2Y35). (B) All known structures of Dcp2, superposed on the Dcp2 regulatory domain and Dcp1 (when present). The Dcp2 catalytic domain (light green) and the catalytic Nudix helix (red) can adopt a large number of orientations with respect to the regulatory domain. In solution, an open, closed and active orientation have been observed (PDB ID 2QKL, 5N2V). (C) Static structures of Xrn1 (PDB ID 2Y35, 6Q8Y), as well as NMR data on Xrn2, reveal motions in the N-terminal helix (red) that correlate with substrate turnover. The stacking interactions between the three most 5′ bases of the substrate RNA (orange) and the conserved His and Trp residues in Xrn1 (blue) are shown.

second RecA domain of the helicase DDX6/Dhh1 (Sharif et al. 2013; Tritschler et al. 2009a) (Figure 3A, purple). Thereby, this latter interaction directly couples decapping (Figure 3) and deadenylation (Figure 2), as DDX6 can simultaneously interact with Edc3 and the Ccr4-Not scaffold protein Not1 (Mathys et al. 2014) (Figure 3A, light blue). However, it remains unclear how the Ccr4-Not complex dissociates from the mRNA to allow for the recruitment of the Lsm1-7 ring, and what the trigger for this exchange is.

The Dcp2 decapping enzyme (Figure 3A, green) contains a catalytic domain with a Nudix helix as well as an N-terminal regulatory domain. This latter domain forms part of the composite substrate binding site (Floor et al. 2010) and interacts tightly with the prime activator of decapping Dcp1 (She et al. 2008) (Figure 3A, yellow). The role of Dcp1 is threefold: first, it stabilizes the N-terminal domain of Dcp2 and thereby facilitates mRNA decapping (Wurm et al. 2017); second, it recruits the Edc1 protein (Figure 3A, pink) that stabilizes the Dcp2 enzyme in an active conformation (Charenton et al. 2016; Mugridge et al. 2018; Wurm et al. 2017); and finally, it provides a dynamic binding groove for proline rich sequences in mRNA decapping factors (Wurm et al. 2016) and Xrn1 (Braun et al. 2012) (Figure 3A, light brown). This latter interaction places the 5′→3′ exoribonuclease close to the decapped transcript, favouring a rapid and processive degradation of the mRNA body after decapping (Chang et al. 2011; Jinek et al. 2011). Xrn1-mediated degradation can also occur on transcripts that are still being actively transcribed, as is

captured in a structure of Xrn1 in complex with the ribosome (Hu et al. 2009; Tesina et al. 2019). Structurally, Xrn1 contains a catalytic core in which the active site pocket is selective for 5′ mono-phosphorylated RNA and thereby strongly discriminates against capped RNA. This Xrn1 core is succeeded by four folded domains whose functions are not well understood. These additional domains are resolved and visible only in some of the determined Xrn1 structures (Chang et al. 2011; Jinek et al. 2011; Tesina et al. 2019), indicating that they can adopt different orientations with respect to the core domain.

The "model" of the 5′→3′ mRNA decay pathway depicted in Figure 3 should not be considered the only possible link between deadenylation and 5′→3′ mRNA degradation. It is important to realize that, similar to the Ccr4-Not deadenylation complex, the domain organization and the interaction details between the different 5′→3′ mRNA decay factors can vary between species. Differences include for example the direct and stable interaction of the Dcp1 and Dcp2 proteins in yeast, whereas in humans the additional protein Edc4 is required to form a functional decapping complex (Jinek et al. 2008). In addition, the yeast Dcp1 protein comprises only one modular domain, while this decapping factor trimerizes in humans via a long C-terminal extension (Tritschler et al. 2009b). Furthermore, the C-terminal IDR of mammalian Xrn1 has been shown to interact not only with Dcp1, but also directly with the Edc4 protein and with Pat1 (Chang et al. 2019). Future structural studies will be needed to reveal how these differences result in species, tissue or cellular conditional differences in the architecture and regulation of the mRNA degradation pathways.

The catalytic domain of Dcp2 possesses only a low intrinsic decapping efficiency that is enhanced by the Dcp2 regulatory domain and regulated by the Dcp2 IDR (He and Jacobson 2015; Paquette et al. 2018). In addition, Dcp2 decapping activity is increased by the interaction with various decapping factors, including Dcp1, Edc1, Edc3, Pat1 and Dhh1 (Nissan et al. 2010; Wurm et al. 2017). It has been experimentally shown that the Dcp1-Dcp2 complex is highly dynamic and that the catalytic domain can adopt different orientations with respect to the rigid conformation that is adopted in the complex of Dcp1 with the Dcp2 regulatory domain (Charenton et al. 2016; Mugridge et al. 2018; She et al. 2006, 2008; Wurm et al. 2017) (Figure 3B). So far, structural studies have described seven different Dcp2 conformations, of which only three have been directly observed in solution (Wurm et al. 2017): an open state that has a high affinity for the body of the RNA substrate, a closed state that is catalytically impaired, and an active state in which mRNA decapping can take place (Figure 3B). The motions in the Dcp2 enzyme have been quantified in detail using high resolution nuclear magnetic resonance (NMR) methods that thereby complement static structural information (Krempl et al. 2022; Wurm et al. 2017). The binding of the decapping activator Edc1 stabilizes the active conformation of Dcp2 and thereby enhances decapping activity directly through the modulation of protein motions (Charenton et al. 2016; Wurm et al. 2017). The regulation of enzyme activity through the modulation of the conformational space that a protein samples is likely a more general mechanism and could also be important for other complexes involved in mRNA turnover. If and how the Dcp2 enzyme is differentially active on cap0, cap1 or other cap structures has not been addressed in detail as far as we are aware, but modifications on or close to the cap structure could influence decapping and thereby provide a means to influence mRNA stability.

The proteins involved in 5′→3′ mRNA decay can condensate into cellular processing bodies, or P-bodies (Sheth and Parker 2003), through a large dynamic network of redundant and weak intermolecular interactions (Li et al. 2012) that involve RNA, folded protein domains as well as disordered protein regions (Fromm et al. 2014; Luo et al. 2018; Schütz et al. 2017). The exact functional role of this self-assembly process remains a matter of debate and it is not clear if processing bodies are sites where mRNA is stably stored, or where active mRNA turnover takes place. It is tempting to speculate that the Dcp2 domain orientation (Figure 3B) is modulated upon condensation such that decapping can be inhibited or enhanced (Damman et al. 2019; Schütz et al. 2017; Tibble et al. 2021).

The importance of structural changes in enzyme function is further illustrated by the Xrn1 enzyme (Figure 3C). The three most 5′ bases of the decapped mRNA stack tightly between a pair of conserved histidine and tryptophan residues to prevent the premature release of the substrate from the enzyme. At the same time, the substrate needs to translocate one base towards the active site after each cleavage event. This substrate movement appears to go in concert with motions in the N-terminal Xrn1 helix (Figure 3C), as structurally different Xrn1 conformations have been observed in static structures of Xrn1 that differ in the translocation step of the substrate (Jinek et al. 2011; Tesina et al. 2019). Experimentally, the link between these motions and enzyme turnover rates has been characterized in solution for the closely related Xrn2 enzyme (Overbeck et al. 2022).

4.2 mRNA turnover step 3b: exosome-mediated degradation of the mRNA body

In mammals, mRNAs appear to be primarily degraded in the 3′→5′ direction (Wang and Kiledjian 2001). In this decay pathway the deadenylated transcripts recruit the cytoplasmic exosome complex that processively degrades the mRNA body.

The central unit of the exosome complex is the catalytically inactive 270 kDa Exo9 core. Exo9 contains a hexameric ring structure that is composed of the heterodimeric RNase PH domain proteins Rrp41-Rrp45, Rrp46-Rrp43 and Mtr3-Rrp42 and that is capped with the RNA binding proteins Csl4, Rrp4 and Rrp40 (Figure 4A) (Cvetkovic et al. 2017). The 3′ end of a single stranded RNA substrate can enter the Exo9 barrel via a narrow pore that is formed by the cap proteins (Liu et al. 2006). The Dis3/Rrp44 protein adds catalytic activity to the exosome (Dziembowski et al. 2007) and interacts with the Exo9 barrel on the site opposite the cap to form the Exo10 complex (Figure 4A). This Exo10 complex is found in the nucleus, where it plays a role in RNA processing and decay, as well as in the cytoplasm, where it is involved in mRNA turnover (Januszyk and Lima 2014).

The ~110 kDa Rrp44 enzyme contains two active sites (Figure 4B), one endonuclease site that is located in the N-terminal PIN (Pilus-forming N-terminus) domain (Lebreton et al. 2008), and one exonuclease site that is found in the C-terminal RNB domain. Both active sites have been suggested to cooperate, but how this would mechanistically work remains unclear. The exonuclease site hydrolyses the substrate base-by-base in a highly processive manner (Lorentzen et al. 2008) and details of the enzyme:RNA interaction have been observed in multiple structures of the complex in the presence of substrate. Interestingly, the Rrp44 enzyme

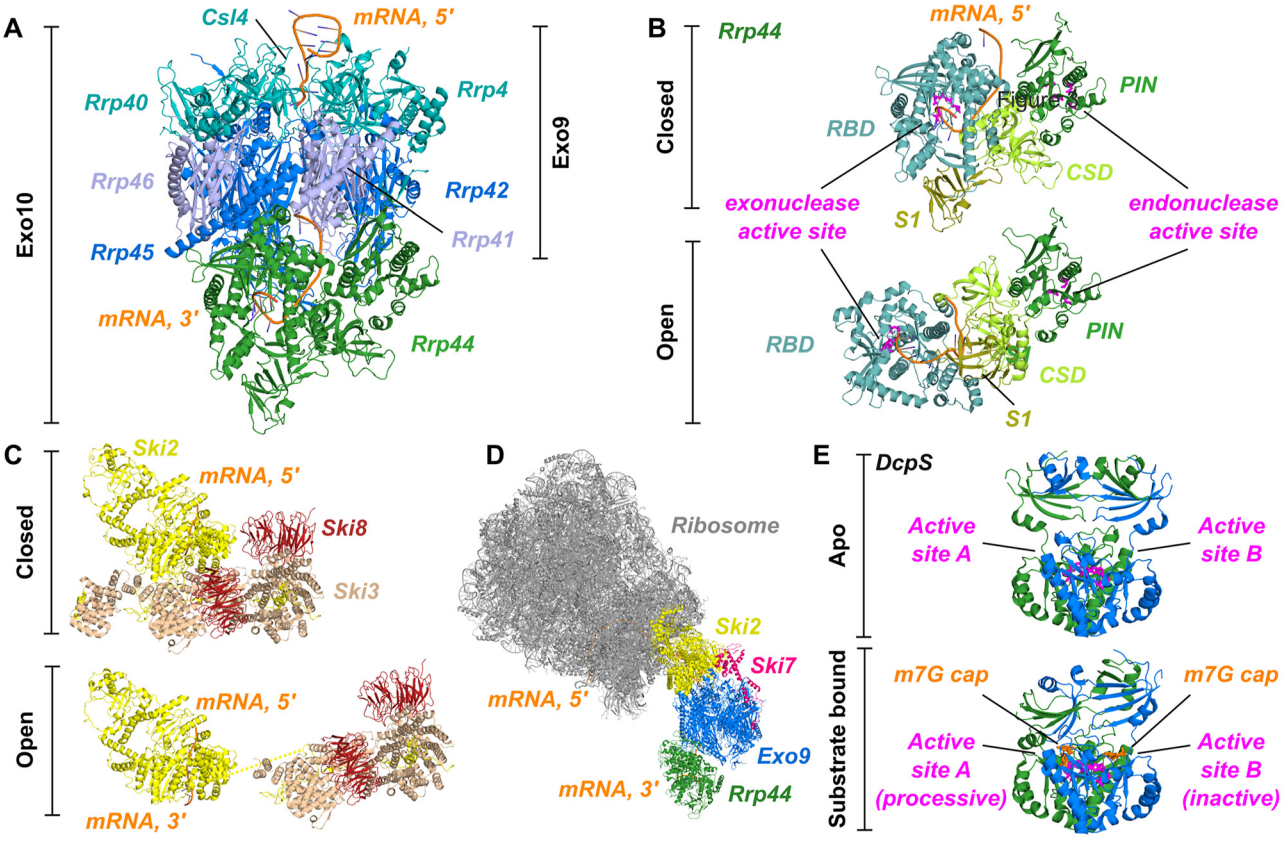

Figure 4: Structures of complexes involved in 3′→5′ mRNA degradation. (A) Structure of the exosome complex (PDB ID 4IFD; Table 4). The central hexameric barrel (dark and light blue) interacts with three cap proteins (teal) that form a narrow entrance channel for the substrate RNA (orange). This Exo9 complex interacts with the catalytic subunit Rrp44 (green) to form Exo10. (B) The Rrp44 enzyme can adopt different conformations that result in different RNA binding grooves. The individual protein domains have been coloured in different shades of green. The exo- and endonuclease active sites are indicated in pink. The image is based on PDB ID 4IFD (top, closed conformation) and 5C0W (bottom, open conformation). (C) The Ski2-3-8 complex can form a closed state (top, PDB ID 7QDY), in which the substrate RNA-binding channel is obstructed by Ski3. The dissociation of the Ski3-8 complex from the Ski2 enzyme opens the RNA channel and allows for the interaction of the Ski complex with Exo10 (PDB ID 7QE0 and 7QDS). (D) Model of how the exosome complex can be recruited to the ribosome in the cytoplasm. The model was constructed by superposing structures of the Ski2-ribosome complex (PDB ID 5MC6), the Ski2 protein in complex with RNA (PDB ID 7QE0) and the Exo10-Ski7 complex (PDB ID 5JEA) onto the structure of the nuclear exosome (PDB ID 6FSZ), structurally aligning Ski2 with Mtr4. (E) Structure of the human DcpS enzyme in the absence (top, PDB ID 1XML) and presence (bottom, PDB ID 1XMM) of substrate. The two DcpS protomers are coloured in green and blue. The catalytic H-x-H-x-H triad is highlighted in pink. The mRNA fragment is shown in orange.

has been observed in two structurally different conformations that differ in domain orientations and RNA binding path (Figure 4B) (Makino et al. 2015). It remains to be determined if and how these large structural changes are linked with the processing activity of the Exo10 complex or with special features in the substrate.

The Exo10 complex interacts with additional factors in a manner that depends on the cellular localization (Januszyk and Lima 2014). In the nucleus, the Exo10 complex associates with the ribonuclease Rrp6, the RNA helicase Mtr4 and the co-factors Rrp47 and Mpp6 (Butler and Mitchell 2011). In the cytoplasm, Exo10 interacts with the adaptor protein Ski7 (Kowalinski et al. 2016; Liu et al. 2016), that can subsequently recruit the SKI (Superkiller) complex, which consists of the RNA helicase Ski2 (structurally highly similar to Mtr4), the tetratricopeptide repeat protein Ski3 and two copies of the WD40 repeat protein Ski8. The recruitment of the SKI complex is essential for exosome-mediated 3′→5′ mRNA decay (Anderson and Parker 1998).

The Ski2-7-8 module has been found in a conformation in which the Ski3-8 proteins block the exit channel of the Ski2 helicase domain, and thereby prevent translocation of the mRNA (Halbach et al. 2013; Kögel et al. 2022) (Figure 4C). In an ATP-dependent manner, the Ski3-8 module can “swing out”, which has two functional consequences. First, the RNA channel in Ski2 opens such that mRNA translocation is no longer obstructed, and second, the helicase domain of Ski2 is then able to dock directly onto the Exo10 complex. The interaction between the Exo10 complex and the Ski-2 helicase domain has not been structurally characterized. However, based on biochemical data and the structure of the nuclear exosome in complex with Mtr4, it is possible to construct a model of the Exo10-Ski7-Ski2 complex (Figure 4D), in which Rrp47 bridges the interaction between the Exo10 complex and Ski2.

The Exo10-SKI complex also plays a role in mRNA surveillance pathways, where faulty mRNA transcripts are endonucleolytically cleaved upon ribosome stalling (Shoemaker and Green 2012). The resulting free 3′ end of the cleaved RNA can then be directly channelled into the exosome via the Ski2 protein (Kögel et al. 2022; Schmidt et al. 2016). Multiple parts of this process have been visualized and can be combined into a structural model (Figure 4D) that shows how the Ski2 protein first interacts with an arch region close to the mRNA exit pore in the ribosome, how afterwards the 3′ end of the mRNA is threaded through the helicase domain of Ski2, and how it then reaches the active site of Rrp44 via the Exo9 complex. At the same time, it remains unclear how the Exo10-SKI complex is targeted to a deadenylated mRNA during canonical mRNA turnover, as no physical link between the deadenylase machinery and the exosome has been identified so far.

The products of the exosomal degradation process are single nucleotides and a small capped RNA fragment of 2–5 nucleotides (Fuchs et al. 2020; Mitchell et al. 1997). These short 5′ cap mRNA fragments are subsequently decapped by the ~80 kDa scavenger decapping enzyme DcpS/Dcs1p, that releases m^7GMP and the 5′ diphosphorylated mRNA fragment (Liu et al. 2002; Nuss and Furuichi 1977; Wang and Kiledjian 2001).

In the apo state, DcpS forms a symmetric homodimer with two active sites, each between the N- and C-terminal lobes (Figure 4E) (Chen et al. 2005). The enzyme undergoes a large structural change upon substrate recruitment, which results in the formation of one catalytically competent active site (Gu et al. 2004). At the same time, the other substrate-binding site opens into an inactive conformation that allows for the concomitant recruitment of a second substrate. Upon hydrolysis of the first substrate, the N-terminal lid domain flips over to form a catalytically competent active site around the second substrate, and consequently releases the products from the first active site. These flipping motions become fast in the presence of a large excess of substrate, thereby inhibiting substrate turnover (Krempl and Sprangers 2023; Neu et al. 2015). Importantly, DcpS is only active on very short mRNA fragments as longer mRNAs prevent the formation of the closed active site due to steric clashes between the enzyme and the third base in the substrate (Fuchs et al. 2020). Functionally, this elegant mechanism prevents the decapping of long mRNAs that might still be actively involved in translation.

An interaction between DcpS and the exosome has been reported (Wang and Kiledjian 2001), although we have not (yet) been able to observe a direct interaction between these complexes *in vitro* using purified components (unpublished data). It thus remains unclear how the exosome products are transferred to DcpS.

5 Variations in the mRNA decay pathways

The steps described above form a basic pathway to facilitate an ordered and regulated turnover of mRNA. Numerous (cell- and organism-dependent) variations to these pathways exist that have not been structurally studied in detail so far. As an example, after deadenylation, or after cleavage of the poly(A) tail, terminal uridylyltransferase enzymes can add 3′ uracil stretches to short poly(A) tails that no longer interact

with Pab1 (Lim et al. 2014). This uridylation results in enhanced mRNA decay rates either through the recruitment of the Lsm1-7 complex and subsequent Dcp2 mediated mRNA decapping (Rissland and Norbury 2009; Song and Kiledjian 2007), or through the action of the Dis3L2 enzyme (Malecki et al. 2013), a paralogue of the Rrp44 enzyme that is unable to associate with the exosome. It remains to be determined under which conditions, and for which substrates, uridylation takes place, and which benefits this may provide.

Likewise, numerous other triggers can lead to the rapid turnover of an mRNA transcript. As described above, the miRNA silencing machinery can directly recruit the Ccr4-Not complex through the TNRC6/GW182 protein or through AU-rich element-binding proteins like TTP. Additional pathways include cellular quality control or surveillance mechanisms that recognize faulty transcripts (Graille and Séraphin 2012), such as those containing a premature translation termination codon (PTC), which activates the nonsense-mediated decay (NMD) pathway (Kervestin and Jacobson 2012) via the translating ribosome. Central to this pathway is the Upf1 (up-frameshift 1) protein that serves at least three functions. First, it interacts with the Dcp2 C-terminal IDR to initiate mRNA decapping; second, it recruits the endoribonuclease SMG6 that cleaves the transcript in the vicinity of the PTC; and, finally, it interacts with the SMG5-SMG7 module, which in turn recruits the Ccr4-Not complex to initiate deadenylation. Similarly, the no-go decay (NGD) pathway (Harigaya and Parker 2010) is activated when ribosomes stall or collide on a transcript, e.g. due to stable secondary structures in the RNA. This can also result in the endoribonucleolytic cleavage of the transcript, followed by the recruitment of the 5′→3′ decay machinery. Analogous to the NGD pathway, the non-stop decay (NSD) pathway (Klauer and van Hoof 2012) is activated when a stop codon is lacking, and translating ribosomes slow down while translating the poly(A) tail (Chandrasekaran et al. 2019; Tesina et al. 2020). In all these cases the same enzymes that play a role in canonical mRNA turnover are recruited via interaction networks that are structurally only partially determined.

6 Concluding remarks

In the past decades our knowledge regarding the structures of the proteins involved in mRNA turnover has increased significantly. Based on that, a picture arises that reveals how these enzymes are embedded in large interaction networks. In the future, it will be important to understand how the activity of these enzymes is regulated on a structural level, which likely involves structural changes and protein dynamics, as was shown for e.g. Dcp2 and the Xrn1 homologue Xrn2. Based on recent technological advances in structural biology methods, including computational methods (Jumper et al. 2021), single-particle cryo-electron microscopy (Guaita et al. 2022) and NMR spectroscopy (Schütz and Sprangers 2019), we are looking forward to exciting future findings that should ultimately allow us to fully describe how mRNA decay is regulated on an atomic level.

Acknowledgments: We would like to thank all lab members for discussions. The authors thank Jan Overbeck, Julian Hübner, David Stelzig and Martin Brehm for constructive comments on the manuscript. The authors would also like to thank Herbert Tschochner for his work as the SFB 960 speaker during the past 12 years.
Research ethics: Not applicable.
Author contributions: All the authors have accepted responsibility for the entire content of this submitted manuscript and approved submission.
Competing interests: The authors declares no conflicts of interest regarding this article.
Research funding: This work was supported by the Deutsche Forschungsgemeinschaft under SFB 960 TP/B12.
Data availability: Not applicable.

References

Absmeier, E., Chandrasekaran, V., O'Reilly, F.J., Stowell, J.A., Rappsilber, J., and Passmore, L.A. (2022). Specific recognition and ubiquitination of slow-moving ribosomes by human CCR4-NOT. preprint from biorxiv.org, https://doi.org/10.1101/2022.07.24.501325.

Aglietti, R.A., Floor, S.N., McClendon, C.L., Jacobson, M.P., and Gross, J.D. (2013). Active site conformational dynamics are coupled to catalysis in the mRNA decapping enzyme Dcp2. Structure 21: 1571–1580.

Anderson, J.S.J. and Parker, R. (1998). The 3' to 5' degradation of yeast mRNAs is a general mechanism for mRNA turnover that requires the SK12 DEVH box protein and 3' to 5' exonucleases of the exosome complex. EMBO J. 17: 1497–1506.

Basquin, J., Roudko, V.V., Rode, M., Basquin, C., Séraphin, B., and Conti, E. (2012). Architecture of the nuclease module of the yeast Ccr4-not complex: the Not1-Caf1-Ccr4 interaction. Mol. Cell 48: 207–218.

Bhandari, D., Raisch, T., Weichenrieder, O., Jonas, S., and Izaurralde, E. (2014). Structural basis for the Nanos-mediated recruitment of the CCR4–NOT complex and translational repression. Genes Dev. 28: 888–901.

Bhaskar, V., Basquin, J., and Conti, E. (2015). Architecture of the ubiquitylation module of the yeast Ccr4-not complex. Structure 23: 921–928.

Bhaskar, V., Roudko, V., Basquin, J., Sharma, K., Urlaub, H., Séraphin, B., and Conti, E. (2013). Structure and RNA-binding properties of the Not1–Not2–Not5 module of the yeast Ccr4–not complex. Nat. Struct. Mol. Biol. 20: 1281–1288.

Boland, A., Chen, Y., Raisch, T., Jonas, S., Kuzuoğlu-Öztürk, D., Wohlbold, L., Weichenrieder, O., and Izaurralde, E. (2013). Structure and assembly of the NOT module of the human CCR4–NOT complex. Nat. Struct. Mol. Biol. 20: 1289–1297.

Bonneau, F., Basquin, J., Ebert, J., Lorentzen, E., and Conti, E. (2009). The yeast exosome functions as a macromolecular cage to channel RNA substrates for degradation. Cell 139: 547–559.

Boo, S.H. and Kim, Y.K. (2020). The emerging role of RNA modifications in the regulation of mRNA stability. Exp. Mol. Med. 52: 400–408.

Brandmann, T., Fakim, H., Padamsi, Z., Youn, J., Gingras, A., Fabian, M.R., and Jinek, M. (2018). Molecular architecture of LSM 14 interactions involved in the assembly of mRNA silencing complexes. EMBO J. 37, https://doi.org/10.15252/embj.201797869.

Braun, J.E., Tritschler, F., Haas, G., Igreja, C., Truffault, V., Weichenrieder, O., and Izaurralde, E. (2010). The C-terminal α–α superhelix of Pat is required for mRNA decapping in metazoa. EMBO J. 29: 2368–2380.

Braun, J.E., Truffault, V., Boland, A., Huntzinger, E., Chang, C.-T., Haas, G., Weichenrieder, O., Coles, M., and Izaurralde, E. (2012). A direct interaction between DCP1 and XRN1 couples mRNA decapping to 5′ exonucleolytic degradation. Nat. Struct. Mol. Biol. 19: 1324–1331.

Brown, C.E. and Sachs, A.B. (1998). Poly(A) tail length control in Saccharomyces cerevisiae occurs by message-specific deadenylation. Mol. Cell. Biol. 18: 6548–6559.

Buschauer, R., Matsuo, Y., Sugiyama, T., Chen, Y.-H., Alhusaini, N., Sweet, T., Ikeuchi, K., Cheng, J., Matsuki, Y., Nobuta, R., et al. (2020). The Ccr4-Not complex monitors the translating ribosome for codon optimality. Science 368: eaay6912.

Butler, J.S. and Mitchell, P. (2011). Rrp6, rrp47 and cofactors of the nuclear exosome. Adv. Exp. Med. Biol. 702: 91–104.

Cesaro, G., Carneiro, F.R.G., Ávila, A.R., Zanchin, N.I.T., and Guimarães, B.G. (2019). Trypanosoma brucei RRP44 is involved in an early stage of large ribosomal subunit RNA maturation. RNA Biol. 16: 133–143.

Cesaro, G., da Soler, H.T., Guerra-Slompo, E.P., Haouz, A., Legrand, P., Zanchin, N.I.T., and Guimaraes, B.G. (2023). *Trypanosoma brucei* RRP44: a versatile enzyme for processing structured and non-structured RNA substrates. Nucleic Acids Res. 51: 380–395.

Chandrasekaran, V., Juszkiewicz, S., Choi, J., Puglisi, J.D., Brown, A., Shao, S., Ramakrishnan, V., and Hegde, R.S. (2019). Mechanism of ribosome stalling during translation of a poly(A) tail. Nat. Struct. Mol. Biol. 26: 1132–1140.

Chang, J.H., Xiang, S., Xiang, K., Manley, J.L., and Tong, L. (2011). Structural and biochemical studies of the 5′→3′ exoribonuclease Xrn1. Nat. Struct. Mol. Biol. 18: 270–276.

Chang, C.-T., Muthukumar, S., Weber, R., Levdansky, Y., Chen, Y., Bhandari, D., Igreja, C., Wohlbold, L., Valkov, E., and Izaurralde, E. (2019). A low-complexity region in human XRN1 directly recruits deadenylation and decapping factors in 5′–3′ messenger RNA decay. Nucleic Acids Res. 47: 9282–9295.

Charenton, C., Taverniti, V., Gaudon-Plesse, C., Back, R., Séraphin, B., and Graille, M. (2016). Structure of the active form of Dcp1–Dcp2 decapping enzyme bound to m7GDP and its Edc3 activator. Nat. Struct. Mol. Biol. 23: 982–986.

Charenton, C., Gaudon-Plesse, C., Fourati, Z., Taverniti, V., Back, R., Kolesnikova, O., Séraphin, B., and Graille, M. (2017). A unique surface on Pat1 C-terminal domain directly interacts with Dcp2 decapping enzyme and Xrn1 5′–3′ mRNA exonuclease in yeast. Proc. Natl. Acad. Sci. USA 114: E9493–E9501.

Charenton, C., Gaudon-Plesse, C., Back, R., Ulryck, N., Cosson, L., Séraphin, B., and Graille, M. (2020). Pby1 is a direct partner of the Dcp2 decapping enzyme. Nucleic Acids Res. 48: 6353–6366.

Chen, N., Walsh, M.A., Liu, Y., Parker, R., and Song, H. (2005). Crystal structures of human DcpS in ligand-free and m7GDP-bound forms suggest a dynamic mechanism for scavenger mRNA decapping. J. Mol. Biol. 347: 707–718.

Chen, Y., Boland, A., Kuzuoğlu-Öztürk, D., Bawankar, P., Loh, B., Chang, C.-T., Weichenrieder, O., and Izaurralde, E. (2014). A DDX6-CNOT1 complex and W-binding pockets in CNOT9 reveal direct links between miRNA target recognition and silencing. Mol. Cell 54: 737–750.

Chen, Y., Khazina, E., Izaurralde, E., and Weichenrieder, O. (2021). Crystal structure and functional properties of the human CCR4-CAF1 deadenylase complex. Nucleic Acids Res. 49: 6489–6510.

Cheng, Z., Coller, J., Parker, R., and Song, H. (2005). Crystal structure and functional analysis of DEAD-box protein Dhh1p. RNA 11: 1258–1270.

Chowdhury, A., Mukhopadhyay, J., and Tharun, S. (2007). The decapping activator Lsm1p-7p–Pat1p complex has the intrinsic ability to distinguish between oligoadenylated and polyadenylated RNAs. RNA 13: 998–1016.

Christie, M., Boland, A., Huntzinger, E., Weichenrieder, O., and Izaurralde, E. (2013). Structure of the PAN3 pseudokinase reveals the basis for interactions with the PAN2 deadenylase and the GW182 proteins. Mol. Cell 51: 360–373.

Cvetkovic, M.A., Wurm, J.P., Audin, M.J., Schütz, S., and Sprangers, R. (2017). The Rrp4-exosome complex recruits and channels substrate RNA by a unique mechanism. Nat. Chem. Biol. 13: 522–528.

Damman, R., Schütz, S., Luo, Y., Weingarth, M., Sprangers, R., and Baldus, M. (2019). Atomic-level insight into mRNA processing bodies by combining solid and solution-state NMR spectroscopy. Nat. Commun. 10: 4536.

Decker, C.J. and Parker, R. (1993). A turnover pathway for both stable and unstable mRNAs in yeast: evidence for a requirement for deadenylation. Genes Dev. 7: 1632–1643.

Deshmukh, M.V., Jones, B.N., Quang-Dang, D.-U., Flinders, J., Floor, S.N., Kim, C., Jemielity, J., Kalek, M., Darzynkiewicz, E., and Gross, J.D. (2008). mRNA decapping is promoted by an RNA-binding channel in Dcp2. Mol. Cell 29: 324–336.

Despic, V. and Jaffrey, S.R. (2023). mRNA ageing shapes the Cap2 methylome in mammalian mRNA. Nature 614: 358–366.

Du, Y., An, W., Zhu, X., Sun, Q., Qi, J., and Ye, K. (2020). Cryo-EM structure of 90 S small ribosomal subunit precursors in transition states. Science 369: 1477–1481.

Dziembowski, A., Lorentzen, E., Conti, E., and Séraphin, B. (2007). A single subunit, Dis3, is essentially responsible for yeast exosome core activity. Nat. Struct. Mol. Biol. 14: 15–22.

Eckmann, C.R., Rammelt, C., and Wahle, E. (2011). Control of poly(A) tail length: control of poly(A) tail length. Wiley Interdiscip. Rev. RNA 2: 348–361.

Fabian, M.R., Cieplak, M.K., Frank, F., Morita, M., Green, J., Srikumar, T., Nagar, B., Yamamoto, T., Raught, B., Duchaine, T.F., et al. (2011). miRNA-mediated deadenylation is orchestrated by GW182 through two conserved motifs that interact with CCR4-NOT. Nat. Struct. Mol. Biol. 18: 1211–1217.

Fabian, M.R., Frank, F., Rouya, C., Siddiqui, N., Lai, W.S., Karetnikov, A., Blackshear, P.J., Nagar, B., and Sonenberg, N. (2013). Structural basis for the recruitment of the human CCR4–NOT deadenylase complex by tristetraprolin. Nat. Struct. Mol. Biol. 20: 735–739.

Faehnle, C.R., Walleshauser, J., and Joshua-Tor, L. (2014). Mechanism of Dis3l2 substrate recognition in the Lin28–let-7 pathway. Nature 514: 252–256.

Falk, S., Bonneau, F., Ebert, J., Kögel, A., and Conti, E. (2017). Mpp6 incorporation in the nuclear exosome contributes to RNA channeling through the Mtr4 helicase. Cell Rep. 20: 2279–2286.

Floor, S.N., Jones, B.N., Hernandez, G.A., and Gross, J.D. (2010). A split active site couples cap recognition by Dcp2 to activation. Nat. Struct. Mol. Biol. 17: 1096–1101.

Fourati, Z., Kolesnikova, O., Back, R., Keller, J., Charenton, C., Taverniti, V., Plesse, C.G., Lazar, N., Durand, D., van Tilbeurgh, H., et al. (2014). The C-terminal domain from *S. cerevisiae* Pat1 displays two conserved regions involved in decapping factor recruitment. PLoS One 9: e96828.

Fromm, S.A., Kamenz, J., Nöldeke, E.R., Neu, A., Zocher, G., and Sprangers, R. (2014). *In Vitro* reconstitution of a cellular phase-transition process that involves the mRNA decapping machinery. Angew. Chem. Int. Ed. 53: 7354–7359.

Fromm, S., Truffault, V., Kamenz, J., Braun, J.E., Hoffmann, N., Izaurralde, E., and Sprangers, R. (2012). The structural basis of Edc3- and Scd6-mediated activation of the Dcp1:Dcp2 mRNA decapping complex. EMBO J. 31: 279–290.

Fuchs, A.-L., Neu, A., and Sprangers, R. (2016). A general method for rapid and cost-efficient large-scale production of 5' capped RNA. RNA 22: 1454–1466.

Fuchs, A.-L., Wurm, J.P., Neu, A., and Sprangers, R. (2020). Molecular basis of the selective processing of short mRNA substrates by the DcpS mRNA decapping enzyme. Proc. Natl. Acad. Sci. USA 117: 19237–19244.

Garneau, N.L., Wilusz, J., and Wilusz, C.J. (2007). The highways and byways of mRNA decay. Nat. Rev. Mol. Cell Biol. 8: 113–126.

Gerlach, P., Schuller, J.M., Bonneau, F., Basquin, J., Reichelt, P., Falk, S., and Conti, E. (2018). Distinct and evolutionary conserved structural features of the human nuclear exosome complex. eLife 7: e38686.

Graille, M. and Séraphin, B. (2012). Surveillance pathways rescuing eukaryotic ribosomes lost in translation. Nat. Rev. Mol. Cell Biol. 13: 727–735.

Gu, M., Fabrega, C., Liu, S.-W., Liu, H., Kiledjian, M., and Lima, C.D. (2004). Insights into the structure, mechanism, and regulation of scavenger mRNA decapping activity. Mol. Cell 14: 67–80.

Guaita, M., Watters, S.C., and Loerch, S. (2022). Recent advances and current trends in cryo-electron microscopy. Curr. Opin. Struct. Biol. 77: 102484.

Halbach, F., Reichelt, P., Rode, M., and Conti, E. (2013). The yeast ski complex: crystal structure and RNA channeling to the exosome complex. Cell 154: 814–826.

Han, G.W., Schwarzenbacher, R., McMullan, D., Abdubek, P., Ambing, E., Axelrod, H., Biorac, T., Canaves, J.M., Chiu, H.J., Dai, X., et al. (2005). Crystal structure of an Apo mRNA decapping enzyme (DcpS) from mouse at 1.83 Å resolution. Proteins: Struct., Funct., Bioinf. 60: 797–802.

Harigaya, Y. and Parker, R. (2010). No-go decay: a quality control mechanism for RNA in translation. Wiley Interdiscip. Rev. RNA 1: 132–141.

He, F. and Jacobson, A. (2015). Control of mRNA decapping by positive and negative regulatory elements in the Dcp2 C-terminal domain. RNA 21: 1633–1647.

Hett, E.C., Xu, H., Geoghegan, K.F., Gopalsamy, A., Kyne, R.E., Menard, C.A., Narayanan, A., Parikh, M.D., Liu, S., Roberts, L., et al. (2015). Rational targeting of active-site tyrosine residues using sulfonyl fluoride probes. ACS Chem. Biol. 10: 1094–1098.

Horiuchi, M., Takeuchi, K., Noda, N., Muroya, N., Suzuki, T., Nakamura, T., Kawamura-Tsuzuku, J., Takahasi, K., Yamamoto, T., and Inagaki, F. (2009). Structural basis for the antiproliferative activity of the Tob-hCaf1 complex. J. Biol. Chem. 284: 13244–13255.

Hosoda, N., Funakoshi, Y., Hirasawa, M., Yamagishi, R., Asano, Y., Miyagawa, R., Ogami, K., Tsujimoto, M., and Hoshino, S. (2011). Anti-proliferative protein Tob negatively regulates CPEB3 target by recruiting Caf1 deadenylase: Tob regulates deadenylation of CPEB3 target. EMBO J. 30: 1311–1323.

Hu, W., Sweet, T.J., Chamnongpol, S., Baker, K.E., and Coller, J. (2009). Co-translational mRNA decay in *Saccharomyces cerevisiae*. Nature 461: 225–229.

Jalkanen, A.L., Coleman, S.J., and Wilusz, J. (2014). Determinants and implications of mRNA poly(A) tail size – does this protein make my tail look big? Semin. Cell Dev. Biol. 34: 24–32.

Januszyk, K. and Lima, C.D. (2014). The eukaryotic RNA exosome. Curr. Opin. Struct. Biol. 24: 132–140.

Jinek, M., Coyle, S.M., and Doudna, J.A. (2011). Coupled 5′ nucleotide recognition and processivity in Xrn1-mediated mRNA decay. Mol. Cell 41: 600–608.

Jinek, M., Eulalio, A., Lingel, A., Helms, S., Conti, E., and Izaurralde, E. (2008). The C-terminal region of Ge-1 presents conserved structural features required for P-body localization. RNA 14: 1991–1998.

Jonas, S., Christie, M., Peter, D., Bhandari, D., Loh, B., Huntzinger, E., Weichenrieder, O., and Izaurralde, E. (2014). An asymmetric PAN3 dimer recruits a single PAN2 exonuclease to mediate mRNA deadenylation and decay. Nat. Struct. Mol. Biol. 21: 599–608.

Jumper, J., Evans, R., Pritzel, A., Green, T., Figurnov, M., Ronneberger, O., Tunyasuvunakool, K., Bates, R., Žídek, A., Potapenko, A., et al. (2021). Highly accurate protein structure prediction with AlphaFold. Nature 596: 583–589.

Kervestin, S. and Jacobson, A. (2012). NMD: a multifaceted response to premature translational termination. Nat. Rev. Mol. Cell Biol. 13: 700–712.

Keskeny, C., Raisch, T., Sgromo, A., Igreja, C., Bhandari, D., Weichenrieder, O., and Izaurralde, E. (2019). A conserved CAF40-binding motif in metazoan NOT4 mediates association with the CCR4–NOT complex. Genes Dev. 33: 236–252.

Klauer, A.A. and van Hoof, A. (2012). Degradation of mRNAs that lack a stop codon: a decade of nonstop progress. Wiley Interdiscip. Rev. RNA 3: 649–660.

Kögel, A., Keidel, A., Bonneau, F., Schäfer, I.B., and Conti, E. (2022). The human SKI complex regulates channeling of ribosome-bound RNA to the exosome via an intrinsic gatekeeping mechanism. Mol. Cell 82: 756–769.e8.

Kowalinski, E., Kögel, A., Ebert, J., Reichelt, P., Stegmann, E., Habermann, B., and Conti, E. (2016). Structure of a cytoplasmic 11-subunit RNA exosome complex. Mol. Cell 63: 125–134.

Krempl, C. and Sprangers, R. (2023). Assessing the applicability of ^{19}F labeled tryptophan residues to quantify protein dynamics. J. Biomol. NMR 77: 55–67.

Krempl, C., Wurm, J.P., Beck Erlach, M., Kremer, W., and Sprangers, R. (2022). Insights into the structure of invisible conformations of large methyl group labeled molecular machines from high pressure NMR. J. Mol. Biol. 435, https://doi.org/10.1016/j.jmb.2022.167922.

Kurosaki, T., Popp, M.W., and Maquat, L.E. (2019). Quality and quantity control of gene expression by nonsense-mediated mRNA decay. Nat. Rev. Mol. Cell Biol. 20: 406–420.

Lai, T., Cho, H., Liu, Z., Bowler, M.W., Piao, S., Parker, R., Kim, Y.K., and Song, H. (2012). Structural basis of the PNRC2-mediated link between mRNA surveillance and decapping. Structure 20: 2025–2037.

Lebreton, A., Tomecki, R., Dziembowski, A., and Séraphin, B. (2008). Endonucleolytic RNA cleavage by a eukaryotic exosome. Nature 456: 993–996.

Li, P., Banjade, S., Cheng, H.-C., Kim, S., Chen, B., Guo, L., Llaguno, M., Hollingsworth, J.V., King, D.S., Banani, S.F., et al. (2012). Phase transitions in the assembly of multivalent signalling proteins. Nature 483: 336–340.

Lim, J., Ha, M., Chang, H., Kwon, S.C., Simanshu, D.K., Patel, D.J., and Kim, V.N. (2014). Uridylation by TUT4 and TUT7 marks mRNA for degradation. Cell 159: 1365–1376.

Lima, S.A., Chipman, L.B., Nicholson, A.L., Chen, Y.-H., Yee, B.A., Yeo, G.W., Coller, J., and Pasquinelli, A.E. (2017). Short poly(A) tails are a conserved feature of highly expressed genes. Nat. Struct. Mol. Biol. 24: 1057–1063.

Ling, S.H.M., Decker, C.J., Walsh, M.A., She, M., Parker, R., and Song, H. (2008). Crystal structure of human Edc3 and its functional implications. Mol. Cell. Biol. 28: 5965–5976.

Liu, H., Rodgers, N.D., Jiao, X., and Kiledjian, M. (2002). The scavenger mRNA decapping enzyme DcpS is a member of the HIT family of pyrophosphatases. EMBO J. 21: 4699–4708.

Liu, J.-J., Niu, C.-Y., Wu, Y., Tan, D., Wang, Y., Ye, M.-D., Liu, Y., Zhao, W., Zhou, K., Liu, Q.-S., et al. (2016). CryoEM structure of yeast cytoplasmic exosome complex. Cell Res. 26: 822–837.

Liu, Q., Greimann, J.C., and Lima, C.D. (2006). Reconstitution, activities, and structure of the eukaryotic RNA exosome. Cell 127: 1223–1237.

Lobel, J.H. and Gross, J.D. (2020). Pdc2/Pat1 increases the range of decay factors and RNA bound by the Lsm1–7 complex. RNA 26: 1380–1388.

Lobel, J.H., Tibble, R.W., and Gross, J.D. (2019). Pat1 activates late steps in mRNA decay by multiple mechanisms. Proc. Natl. Acad. Sci. USA 116: 23512–23517.

Lorentzen, E., Basquin, J., Tomecki, R., Dziembowski, A., and Conti, E. (2008). Structure of the active subunit of the yeast exosome core, Rrp44: diverse modes of substrate recruitment in the RNase II nuclease family. Mol. Cell 29: 717–728.

Lowell, J.E., Rudner, D.Z., and Sachs, A.B. (1992). 3'-UTR-dependent deadenylation by the yeast poly(A) nuclease. Genes Dev. 6: 2088–2099.

Luo, Y., Na, Z., and Slavoff, S.A. (2018). P-Bodies: composition, properties, and functions. Biochemistry 57: 2424–2431.

Lv, H., Zhu, Y., Qiu, Y., Niu, L., Teng, M., and Li, X. (2015). Structural analysis of Dis3l2, an exosome-independent exonuclease from Schizosaccharomyces pombe. Acta Crystallogr., Sect. D: Biol. Crystallogr. 71: 1284–1294.

Makino, D.L., Baumgärtner, M., and Conti, E. (2013). Crystal structure of an RNA-bound 11-subunit eukaryotic exosome complex. Nature 495: 70–75.

Makino, D.L., Schuch, B., Stegmann, E., Baumgärtner, M., Basquin, C., and Conti, E. (2015). RNA degradation paths in a 12-subunit nuclear exosome complex. Nature 524: 54–58.

Malecki, M., Viegas, S.C., Carneiro, T., Golik, P., Dressaire, C., Ferreira, M.G., and Arraiano, C.M. (2013). The exoribonuclease Dis3L2 defines a novel eukaryotic RNA degradation pathway. EMBO J. 32: 1842–1854.

Mangus, D.A., Evans, M.C., and Jacobson, A. (2003). Poly(A)-binding proteins: multifunctional scaffolds for the post-transcriptional control of gene expression. Genome Biol. 4: 223.

Mathys, H., Basquin, J., Ozgur, S., Czarnocki-Cieciura, M., Bonneau, F., Aartse, A., Dziembowski, A., Nowotny, M., Conti, E., and Filipowicz, W. (2014). Structural and biochemical insights to the role of the CCR4-NOT complex and DDX6 ATPase in microRNA repression. Mol. Cell 54: 751–765.

Mauxion, F., Basquin, J., Ozgur, S., Rame, M., Albrecht, J., Schäfer, I., Séraphin, B., and Conti, E. (2023). The human CNOT1-CNOT10-CNOT11 complex forms a structural platform for protein-protein interactions. Cell Rep. 42: 111902.

Mitchell, P., Petfalski, E., Shevchenko, A., Mann, M., and Tollervey, D. (1997). The exosome: a conserved eukaryotic RNA processing complex containing multiple 3′→5′ exoribonucleases. Cell 91: 457–466.

Montemayor, E.J., Virta, J.M., Hayes, S.M., Nomura, Y., Brow, D.A., and Butcher, S.E. (2020). Molecular basis for the distinct cellular functions of the Lsm1–7 and Lsm2–8 complexes. RNA 26: 1400–1413.

Mugridge, J.S., Tibble, R.W., Ziemniak, M., Jemielity, J., and Gross, J.D. (2018). Structure of the activated Edc1-Dcp1-Dcp2-Edc3 mRNA decapping complex with substrate analog poised for catalysis. Nat. Commun. 9: 1152.

Mugridge, J.S., Ziemniak, M., Jemielity, J., and Gross, J.D. (2016). Structural basis of mRNA-cap recognition by Dcp1–Dcp2. Nat. Struct. Mol. Biol. 23: 987–994.

Muhlrad, D., Decker, C.J., and Parker, R. (1995). Turnover mechanisms of the stable yeast PGK1 mRNA. Mol. Cell. Biol. 15: 2145–2156.

Mund, M., Neu, A., Ullmann, J., Neu, U., and Sprangers, R. (2011). Structure of the LSm657 complex: an assembly intermediate of the LSm1–7 and LSm2–8 rings. J. Mol. Biol. 414: 165–176.

Naidoo, N., Harrop, S.J., Sobti, M., Haynes, P.A., Szymczyna, B.R., Williamson, J.R., Curmi, P.M.G., and Mabbutt, B.C. (2008). Crystal structure of Lsm3 octamer from *Saccharomyces cerevisiae*: implications for Lsm ring organisation and recruitment. J. Mol. Biol. 377: 1357–1371.

Nasertorabi, F., Batisse, C., Diepholz, M., Suck, D., and Böttcher, B. (2011). Insights into the structure of the CCR4-NOT complex by electron microscopy. FEBS Lett. 585: 2182–2186.

Neu, A., Neu, U., Fuchs, A.-L., Schlager, B., and Sprangers, R. (2015). An excess of catalytically required motions inhibits the scavenger decapping enzyme. Nat. Chem. Biol. 11: 697–704.

Nissan, T., Rajyaguru, P., She, M., Song, H., and Parker, R. (2010). Decapping activators in *Saccharomyces cerevisiae* act by multiple mechanisms. Mol. Cell 39: 773–783.

Nuss, D.L. and Furuichi, Y. (1977). Characterization of the m7G(5') pppN-pyrophosphatase activity from HeLa cells. J. Biol. Chem. 252: 2815–2821.

Overbeck, J.H., Stelzig, D., Fuchs, A.-L., Wurm, J.P., and Sprangers, R. (2022). Observation of conformational changes that underlie the catalytic cycle of Xrn2. Nat. Chem. Biol. 18: 1152–1160.

Ozgur, S., Basquin, J., Kamenska, A., Filipowicz, W., Standart, N., and Conti, E. (2015). Structure of a human 4E-T/DDX6/CNOT1 complex reveals the different interplay of DDX6-binding proteins with the CCR4-NOT complex. Cell Rep. 13: 703–711.

Paquette, D.R., Tibble, R.W., Daifuku, T.S., and Gross, J.D. (2018). Control of mRNA decapping by autoinhibition. Nucleic Acids Res. 46: 6318–6329.

Peter, D., Ruscica, V., Bawankar, P., Weber, R., Helms, S., Valkov, E., Igreja, C., and Izaurralde, E. (2019). Molecular basis for GIGYF–Me31B complex assembly in 4EHP-mediated translational repression. Genes Dev. 33: 1355–1360.

Petit, A.-P., Wohlbold, L., Bawankar, P., Huntzinger, E., Schmidt, S., Izaurralde, E., and Weichenrieder, O. (2012). The structural basis for the interaction between the CAF1 nuclease and the NOT1 scaffold of the human CCR4–NOT deadenylase complex. Nucleic Acids Res. 40: 11058–11072.

Piao, X., Zhang, X., Wu, L., and Belasco, J.G. (2010). CCR4-NOT deadenylates mRNA associated with RNA-induced silencing complexes in human cells. Mol. Cell. Biol. 30: 1486–1494.

Raisch, T., Bhandari, D., Sabath, K., Helms, S., Valkov, E., Weichenrieder, O., and Izaurralde, E. (2016). Distinct modes of recruitment of the CCR 4–NOT complex by Drosophila and vertebrate Nanos. EMBO J. 35: 974–990.

Raisch, T., Chang, C.-T., Levdansky, Y., Muthukumar, S., Raunser, S., and Valkov, E. (2019). Reconstitution of recombinant human CCR4-NOT reveals molecular insights into regulated deadenylation. Nat. Commun. 10: 3173.

Raisch, T., Sandmeir, F., Weichenrieder, O., Valkov, E., and Izaurralde, E. (2018). Structural and biochemical analysis of a NOT1 MIF4G-like domain of the CCR4-NOT complex. J. Struct. Biol. 204: 388–395.

Rissland, O.S. and Norbury, C.J. (2009). Decapping is preceded by 3′ uridylation in a novel pathway of bulk mRNA turnover. Nat. Struct. Mol. Biol. 16: 616–623.

Schäfer, I.B., Rode, M., Bonneau, F., Schüssler, S., and Conti, E. (2014). The structure of the Pan2–Pan3 core complex reveals cross-talk between deadenylase and pseudokinase. Nat. Struct. Mol. Biol. 21: 591–598.

Schäfer, I.B., Yamashita, M., Schuller, J.M., Schüssler, S., Reichelt, P., Strauss, M., and Conti, E. (2019). Molecular basis for poly(A) RNP architecture and recognition by the Pan2-Pan3 deadenylase. Cell 177: 1619–1631.e21.

Schmidt, C., Kowalinski, E., Shanmuganathan, V., Defenouillère, Q., Braunger, K., Heuer, A., Pech, M., Namane, A., Berninghausen, O., Fromont-Racine, M., et al. (2016). The cryo-EM structure of a ribosome–Ski2-Ski3-Ski8 helicase complex. Science 354: 1431–1433.

Schuller, J.M., Falk, S., Fromm, L., Hurt, E., and Conti, E. (2018). Structure of the nuclear exosome captured on a maturing preribosome. Science 360: 219–222.

Schütz, S., Noldeke, E.R., and Sprangers, R. (2017). A synergistic network of interactions promotes the formation of *in vitro* processing bodies and protects mRNA against decapping. Nucleic Acids Res. 45: 6911–6922.

Schütz, S. and Sprangers, R. (2019). Methyl TROSY spectroscopy: a versatile NMR approach to study challenging biological systems. Prog. Nucl. Magn. Reson. Spectrosc. 116: 56–84.

Sgromo, A., Raisch, T., Backhaus, C., Keskeny, C., Alva, V., Weichenrieder, O., and Izaurralde, E. (2018). Drosophila Bag-of-marbles directly interacts with the CAF40 subunit of the CCR4–NOT complex to elicit repression of mRNA targets. RNA 24: 381–395.

Sgromo, A., Raisch, T., Bawankar, P., Bhandari, D., Chen, Y., Kuzuoğlu-Öztürk, D., Weichenrieder, O., and Izaurralde, E. (2017). A CAF40-binding motif facilitates recruitment of the CCR4-NOT complex to mRNAs targeted by Drosophila Roquin. Nat. Commun. 8: 14307.

Sharif, H. and Conti, E. (2013). Architecture of the Lsm1-7-Pat1 complex: a conserved assembly in eukaryotic mRNA turnover. Cell Rep. 5: 283–291.

Sharif, H., Ozgur, S., Sharma, K., Basquin, C., Urlaub, H., and Conti, E. (2013). Structural analysis of the yeast Dhh1-Pat1 complex reveals how Dhh1 engages Pat1, Edc3 and RNA in mutually exclusive interactions. Nucleic Acids Res. 41: 8377–8390.

Shatkin, A. (1976). Capping of eucaryotic mRNAs. Cell 9: 645–653.

She, M., Decker, C.J., Chen, N., Tumati, S., Parker, R., and Song, H. (2006). Crystal structure and functional analysis of Dcp2p from *Schizosaccharomyces pombe*. Nat. Struct. Mol. Biol. 13: 63–70.

She, M., Decker, C.J., Sundramurthy, K., Liu, Y., Chen, N., Parker, R., and Song, H. (2004). Crystal structure of Dcp1p and its functional implications in mRNA decapping. Nat. Struct. Mol. Biol. 11: 249–256.

She, M., Decker, C.J., Svergun, D.I., Round, A., Chen, N., Muhlrad, D., Parker, R., and Song, H. (2008). Structural basis of Dcp2 recognition and activation by Dcp1. Mol. Cell 29: 337–349.

Sheth, U. and Parker, R. (2003). Decapping and decay of messenger RNA occur in cytoplasmic processing bodies. Science 300: 805–808.

Shoemaker, C.J. and Green, R. (2012). Translation drives mRNA quality control. Nat. Struct. Mol. Biol. 19: 594–601.

Siddiqui, N., Mangus, D.A., Chang, T.-C., Palermino, J.-M., Shyu, A.-B., and Gehring, K. (2007). Poly(A) nuclease interacts with the C-terminal domain of polyadenylate-binding protein domain from poly(A)-binding protein. J. Biol. Chem. 282: 25067–25075.

Singh, J., Salcius, M., Liu, S.-W., Staker, B.L., Mishra, R., Thurmond, J., Michaud, G., Mattoon, D.R., Printen, J., Christensen, J., et al. (2008). DcpS as a therapeutic target for spinal muscular atrophy. ACS Chem. Biol. 3: 711–722.

Song, M.-G. and Kiledjian, M. (2007). 3′ Terminal oligo U-tract-mediated stimulation of decapping. RNA 13: 2356–2365.

Tang, T.T.L., Stowell, J.A.W., Hill, C.H., and Passmore, L.A. (2019). The intrinsic structure of poly(A) RNA determines the specificity of Pan2 and Caf1 deadenylases. Nat. Struct. Mol. Biol. 26: 433–442.

Tesina, P., Heckel, E., Cheng, J., Fromont-Racine, M., Buschauer, R., Kater, L., Beatrix, B., Berninghausen, O., Jacquier, A., Becker, T., et al. (2019). Structure of the 80S ribosome-Xrn1 nuclease complex. Nat. Struct. Mol. Biol. 26: 275–280.

Tesina, P., Lessen, L.N., Buschauer, R., Cheng, J., Wu, C.C.-C., Berninghausen, O., Buskirk, A.R., Becker, T., Beckmann, R., and Green, R. (2020). Molecular mechanism of translational stalling by inhibitory codon combinations and poly(A) tracts. EMBO J. 39: e103365.

Tharun, S. and Parker, R. (2001). Targeting an mRNA for decapping: displacement of translation factors and association of the Lsm1p-7p complex on deadenylated yeast mRNAs. Mol. Cell 8: 1075–1083.

Tibble, R.W., Depaix, A., Kowalska, J., Jemielity, J., and Gross, J.D. (2021). Biomolecular condensates amplify mRNA decapping by biasing enzyme conformation. Nat. Chem. Biol. 17: 615–623.

Tritschler, F., Braun, J.E., Eulalio, A., Truffault, V., Izaurralde, E., and Weichenrieder, O. (2009a). Structural basis for the mutually exclusive anchoring of P body components EDC3 and Tral to the DEAD box protein DDX6/Me31B. Mol. Cell 33: 661–668.

Tritschler, F., Braun, J.E., Motz, C., Igreja, C., Haas, G., Truffault, V., Izaurralde, E., and Weichenrieder, O. (2009b). DCP1 forms asymmetric trimers to assemble into active mRNA decapping complexes in metazoa. Proc. Natl. Acad. Sci. USA 106: 21591–21596.

Tritschler, F., Eulalio, A., Truffault, V., Hartmann, M.D., Helms, S., Schmidt, S., Coles, M., Izaurralde, E., and Weichenrieder, O. (2007). A divergent Sm fold in EDC3 proteins mediates DCP1 binding and P-body targeting. Mol. Cell. Biol. 27: 8600–8611.

Tucker, M., Valencia-Sanchez, M.A., Staples, R.R., Chen, J., Denis, C.L., and Parker, R. (2001). The transcription factor associated Ccr4 and Caf1 proteins are components of the major cytoplasmic mRNA deadenylase in *Saccharomyces cerevisiae*. Cell 104: 377–386.

Uchida, N., Hoshino, S.-I., and Katada, T. (2004). Identification of a human cytoplasmic poly(A) nuclease complex stimulated by poly(A)-binding protein. J. Biol. Chem. 279: 1383–1391.

Valkov, E., Muthukumar, S., Chang, C.-T., Jonas, S., Weichenrieder, O., and Izaurralde, E. (2016). Structure of the Dcp2–Dcp1 mRNA-decapping complex in the activated conformation. Nat. Struct. Mol. Biol. 23: 574–579.

Wang, H., Morita, M., Yang, X., Suzuki, T., Yang, W., Wang, J., Ito, K., Wang, Q., Zhao, C., Bartlam, M., et al. (2010). Crystal structure of the human CNOT6L nuclease domain reveals strict poly(A) substrate specificity. EMBO J. 29: 2566–2576.

Wang, Y., Liu, C.L., Storey, J.D., Tibshirani, R.J., Herschlag, D., and Brown, P.O. (2002). Precision and functional specificity in mRNA decay. Proc. Natl. Acad. Sci. USA 99: 5860–5865.

Wang, Z. and Kiledjian, M. (2001). Functional link between the mammalian exosome and mRNA decapping. Cell 107: 751–762.

Wasmuth, E.V., Januszyk, K., and Lima, C.D. (2014). Structure of an Rrp6–RNA exosome complex bound to poly(A) RNA. Nature 511: 435–439.

Wasmuth, E.V., Zinder, J.C., Zattas, D., Das, M., and Lima, C.D. (2017). Structure and reconstitution of yeast Mpp6-nuclear exosome complexes reveals that Mpp6 stimulates RNA decay and recruits the Mtr4 helicase. eLife 6: e29062.

Weick, E.-M., Puno, M.R., Januszyk, K., Zinder, J.C., DiMattia, M.A., and Lima, C.D. (2018). Helicase-dependent RNA decay illuminated by a cryo-EM structure of a human nuclear RNA exosome-MTR4 complex. Cell 173: 1663–1677.e21.

Wojtczak, B.A., Sikorski, P.J., Fac-Dabrowska, K., Nowicka, A., Warminski, M., Kubacka, D., Nowak, E., Nowotny, M., Kowalska, J., and Jemielity, J. (2018). 5′-Phosphorothiolate dinucleotide cap analogues: reagents for messenger RNA modification and potent small-molecular inhibitors of decapping enzymes. J. Am. Chem. Soc. 140: 5987–5999.

Wolf, J., Valkov, E., Allen, M.D., Meineke, B., Gordiyenko, Y., Mclaughlin, S.H., Olsen, T.M., Robinson, C.V., Bycroft, M., Stewart, M., et al. (2014). Structural basis for Pan3 binding to Pan2 and its function in mRNA recruitment and deadenylation. EMBO J. 33: 1514–1526.

Wu, D., Jiang, S., Bowler, M.W., and Song, H. (2012). Crystal structures of Lsm3, Lsm4 and Lsm5/6/7 from *Schizosaccharomyces pombe*. PLoS One 7: e36768.

Wu, D., Muhlrad, D., Bowler, M.W., Jiang, S., Liu, Z., Parker, R., and Song, H. (2014). Lsm2 and Lsm3 bridge the interaction of the Lsm1-7 complex with Pat1 for decapping activation. Cell Res. 24: 233–246.

Wu, M., Reuter, M., Lilie, H., Liu, Y., Wahle, E., and Song, H. (2005). Structural insight into poly(A) binding and catalytic mechanism of human PARN: crystal structure of PARN. EMBO J. 24: 4082–4093.

Wurm, J.P., Holdermann, I., Overbeck, J.H., Mayer, P.H.O., and Sprangers, R. (2017). Changes in conformational equilibria regulate the activity of the Dcp2 decapping enzyme. Proc. Natl. Acad. Sci. USA 114: 6034–6039.

Wurm, J.P., Overbeck, J., and Sprangers, R. (2016). The S. pombe mRNA decapping complex recruits cofactors and an Edc1-like activator through a single dynamic surface. RNA 22: 1360–1372.

Xu, N., Chen, C.Y., and Shyu, A.B. (1997). Modulation of the fate of cytoplasmic mRNA by AU-rich elements: key sequence features controlling mRNA deadenylation and decay. Mol. Cell. Biol. 17: 4611–4621.

Yamashita, A., Chang, T.-C., Yamashita, Y., Zhu, W., Zhong, Z., Chen, C.-Y.A., and Shyu, A.-B. (2005). Concerted action of poly(A) nucleases and decapping enzyme in mammalian mRNA turnover. Nat. Struct. Mol. Biol. 12: 1054–1063.

Yang, E., Nimwegen, E.V., Zavolan, M., Rajewsky, N., Schroeder, M., Magnasco, M., and Darnell, J.E. (2003). Decay rates of human mRNAs: correlation with functional characteristics and sequence attributes. Genome Res. 13: 1863–1872.

Zhang, Q., Pavanello, L., Potapov, A., Bartlam, M., and Winkler, G.S. (2022). Structure of the human Ccr4-Not nuclease module using X-ray crystallography and electron paramagnetic resonance spectroscopy distance measurements. Protein Sci. 31: 758–764.

Zhou, L., Hang, J., Zhou, Y., Wan, R., Lu, G., Yin, P., Yan, C., and Shi, Y. (2014). Crystal structures of the Lsm complex bound to the 3′ end sequence of U6 small nuclear RNA. Nature 506: 116–120.

Zinder, J.C., Wasmuth, E.V., and Lima, C.D. (2016). Nuclear RNA exosome at 3.1 Å reveals substrate specificities, RNA paths, and allosteric inhibition of Rrp44/Dis3. Mol. Cell 64: 734–745.